Resources Chemicals and Materials 1 (2022) 47–68

Contents lists available at ScienceDirect

Resources Chemicals and Materials

journal homepage: www.elsevier.com/locate/recm

# Catalytic conversion of bioethanol to value-added chemicals and fuels: A review

Huan Xiang[a,b,1], Ruojia Xin[a,1], Natthawan Prasongthum[c], Paweesuda Natewong[d], Tawan Sooknoi[e], Jiawei Wang[b], Prasert Reubroycharoen[f,*], Xiaolei Fan[a,*]

[a] Department of Chemical Engineering and Analytical Science, School of Engineering, The University of Manchester, Manchester M13 9PL, United Kingdom
[b] Department of Chemical Engineering and Applied Chemistry, Aston University, Birmingham, B4 7ET, United Kingdom
[c] Expert Centre of Innovative Clean Energy and Environment, Thailand Institute of Scientific and Technological Research (TISTR), 35 Mu 3, Khlong Ha, Khlong Luang, Pathum Thani 12120, Thailand
[d] Clean Energy Technologies Research Institute (CETRI), Faculty of Engineering & Applied Science, University of Regina, Regina, Saskatchewan, S4S0A2, Canada
[e] Department of Chemistry, Faculty of Science, King Mongkut's Institute of Technology Ladkrabang, Bangkok 10520, Thailand
[f] Center of Excellence in Catalysis for Bioenergy and Renewable Chemicals (CBRC), Faculty of Science, Chulalongkorn University, Bangkok 10330, Thailand

ARTICLE INFO

*Keywords:*
Bioethanol
Catalysis
Hydrogen, $C_2$–$C_4$ olefins
Gasoline
Oxygenates

ABSTRACT

Bioethanol produced *via* valorisation of renewable biomass is of great interest to many industries. The increased availability and decreased cost of bioethanol make it a promising platform molecule to produce a wide range of value-added chemicals and fuels *via* the catalytic conversions. This paper provides a comprehensive review of catalytic conversions of bioethanol to a variety of chemicals/fuels such as hydrogen, $C_2$–$C_4$ olefins, gasoline and small oxygenates. Specifically, the focus was placed on the relationship between the catalyst property (such as pore structure, acidity, active metal sites, and catalyst supports) and the catalytic performance (including catalyst activity and stability), as well as the reaction mechanisms involved. Future research avenues on the catalyst design for improving catalytic valorisation of bioethanol are also discussed.

## 1. Introduction

The rising demand for energy around the world caused the extensive use of fossil fuels, leading to environmental issues, such as climate changes, global warming, and air pollution [1,2]. Therefore, the development of renewable and sustainable energy sources has attracted great attention from the scientific community. Biofuels, such as biodiesel and bioethanol, produced from biomass valorisation, are now considered as promising alternatives to the fossil fuels due to their environmental-friendly and sustainable features. In the United States (US), the Energy Independence and Security Act announced that the renewable fuels used by transportation need to increase to 36 billion gallons per year by 2022 [3,4]. The Biofuels Research advisory Council of European Union (EU) proposed increasing the use of biofuels in transportation to 25% by 2030 [5]. The biofuel policies in US and EU aim to reduce greenhouse gas emissions, improve the life cycle energy efficiency of biofuels, and promote the national biofuel industry (*i.e.,* the production of biofuels including bioethanol, biobutanol, and biodiesel). In Asia, the production and use of biofuels are also widely encouraged. For example, in 2017, the Chinese government announced to roll out the mandatory blending of 10% ethanol in gasoline nationally by 2020 [6]. To meet the target, significant development has been made to enhance the bioethanol production capacity. In Association of Southeast Asian Nation (ASEAN), biofuel policies are robust because domestic biofuel consumption is a means for energy security while promoting socio-economic development through ensuring the demand for strategically critical agricultural commodities [7]. As one of the ASEAN member states, Thailand has also set a target to increase bioethanol production from 6.2 million litres per day in 2016 to 9.0 million litres per day in 2022 to reduce greenhouse gas emission and fossil fuel dependency [8]. The world production of bioethanol was 110 billion litres (BL) in 2018 and is expected to reach 140 BL in 2022 [9]. In addition, the market of bioethanol fuel has shown a dramatic increase and growing at a compound annual growth rate of 7.6% from 2016 to 2022.

*Abbreviations:* SR, Steam reforming; ESR, Ethanol steam reforming; WGS, Water gas shift; TPD, Temperature programmed desorption; AC, Activated carbon; CNT, Carbon nanotube; CNF, Carbon nanofibre; ETE, Ethanol-to-ethylene; DEE, Diethyl ether; ETP, Ethanol-to-propylene; MPV, Meerwein-Ponndorf-Verley; BD, 1,3-Butadiene; TOS, Time-on-stream; ETG, Ethanol-to-gasoline; MTG, Methanol-to-gasoline; BTX, Benzene toluene xylene; HAP, Hydroxyapatite; CHAP, Carbonate hydroxyapatite.

* Corresponding authors.
*E-mail addresses:* prasert.r@chula.ac.th (P. Reubroycharoen), Xiaolei.fan@manchester.ac.uk (X. Fan).

[1] These authors contributed equally to this work.

https://doi.org/10.1016/j.recm.2021.12.002
Received 27 July 2021; Received in revised form 21 November 2021; Accepted 6 December 2021

Bioethanol is a natural type of ethanol made by fermenting the sugar and starch components of plant by-products including sugarcane, corn, and wheat. Since it can be produced directly from renewable biomass, it shows a sustainable feature. Bioethanol has higher octane number (~113) than that of gasoline (usually <100). A higher octane number of a fuel means less volatility and higher compression, so the fuel doesn't ignite too early in the cycle (*i.e.*, the fuel has greater resistance to knock). Besides, bioethanol is biodegradable and less toxic than fossil fuels. Bioethanol is one of the most common biofuels, and it accounts for almost 90% of global biofuel production [10]. Bioethanol can be integrated into the existing road transport fuel system without the need of engine modifications. For example, it can be used in petrol engines as the gasoline additive. Bioethanol can also be used as fuel for power generation by thermal combustion and for fuel cells by thermochemical reactions. In addition, it can also be used as feedstock in chemical industry.

Currently, three generations of bioethanol were developed, depending on different feedstocks. The first-generation bioethanol is produced through fermentation of glucose contained in starch and sugar crops [11,12]. Corn and sugarcane are the main sources in the US and Brazil, while wheat and sugar beet are common in Europe [13]. Since all the feedstocks are edible crops, production of the first-generation bioethanol is a potential threat to food supply. Consequently, the second-generation bioethanol derived from lignocellulosic materials (*e.g.* corn stover, wheat straw, and sugarcane bagasse [14]) emerged to overcome the food *versus* fuel dilemma faced by the first-generation bioethanol. The advantage of the second-generation bioethanol is evident due to the ready availability of the feedstock, which does not compete with the food. However, compared to the first-generation bioethanol, the production of second-generation bioethanol requires additional processes, *i.e.*, lignocellulose needs to be pre-treated first to obtain fermentable substrates (sugars and starch) [11,15]. Therefore, cost-effective production of fermentable sugars from lignocellulosic biomass remains a challenge. The third-generation bioethanol is based on the use of marine organisms, such as algae. Algal biomass has high carbohydrate contents, and it is easy to be cultivated in aqueous environments. The low land usage of algal biomass can limit the feedstock competition with the agriculture plants, making it a potential alternative feedstock for commercial bioethanol production [13]. However, the research on the third-generation bioethanol is still in the early stage due to the limited investments and difficulties in the process design.

Although ethanol is produced worldwide (Fig. 1), the US and Brazil are the leading ethanol producing countries, being responsible for approximately 84% of global production in 2020 [16]. The annual production of bioethanol is constantly increasing. Currently, the most widespread use of bioethanol is in fuel production (*e.g.*, as gasoline additive). Adding a proportion of bioethanol to conventional gasoline can reduce greenhouse gas emission during combustion. Blending gasoline with bioethanol is compatible to conventional infrastructures (*e.g.*, combustion engine) and has been mandated to substitute part of fossil fuels for transportation. However, the blending ratio is only limited to 5–10 vol.% (E5–E10) in the US [17]. The low blending ratio is mainly due to the inherent corrosive nature of bioethanol, which can damage many engine components. The annual bioethanol production in the US has went beyond the blending wall of E10 in 2014 [10]. Besides, higher blending ratio (*e.g.*, E15–E20) and even ethanol-enriched fuels (*e.g.*, E80) are not likely to be widely practiced due to the concerns about fuel economy and severe damage to the conventional engine. Therefore, alternative applications are needed to utilise bioethanol for valorisation.

In addition to be used as gasoline additive/alternative, bioethanol can also be regarded as a platform molecule for making other value-added chemicals/fuels, such as hydrogen ($H_2$) [18], light olefins [19–22], high alcohols [23], gasoline [24], and other small oxygenates (*e.g.*, acetaldehyde, diethyl ether, and acetic acid) [25,26]. Hydrogen is a clean energy source and can be used for ammonia production, petroleum refining, welding, and fuel cells. Light olefins are important building blocks for many modern plastic and rubber products. High alcohols are widely used as solvent in pharmaceuticals and cosmetics. Small oxygenates can be used as solvent and substrate to produce many other chemicals.

Catalysts are generally required to enable the conversion of bioethanol to the chemicals/fuels above, *i.e.*, catalytic conversion of bioethanol. Common catalysts used for the conversions are zeolites, metal oxides, and supported metal catalysts [10,27]. The type of catalysts varies depending on the target product because the derivation of different products from bioethanol go through different chemistry. During the past decade, many studies have been carried out to develop conversion technologies to derive ethanol to other useful chemicals, as summarized by the following review articles. Abdulrazzaq et al. [27] and Dagle *et al.* [28] reviewed the catalytic conversion of ethanol to commodity and specialty chemicals (including $C_2$–$C_4$ olefins, acetaldehyde, diethyl ether, acetone, acetic acid, ethyl acetate, and higher alcohols). Vaidya et al. reviewed the kinetics of ethanol steam reforming for hydrogen production [29] and the recent progress of ethanol steam reforming using non-noble transition metal catalysts were discussed by Ogo et al. [30]. Eagan et al. summarised the chemistries and processes for the conversion of ethanol into middle-distillate fuels [4]. Additionally, few reviews also focus specifically on bioethanol conversion. For

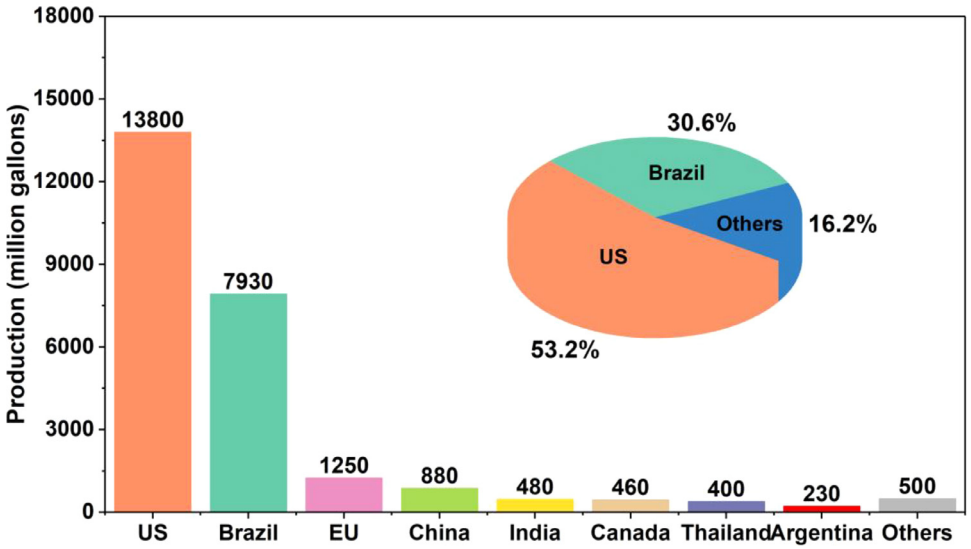


**Fig. 1.** Ethanol production around the world in 2020 [16].

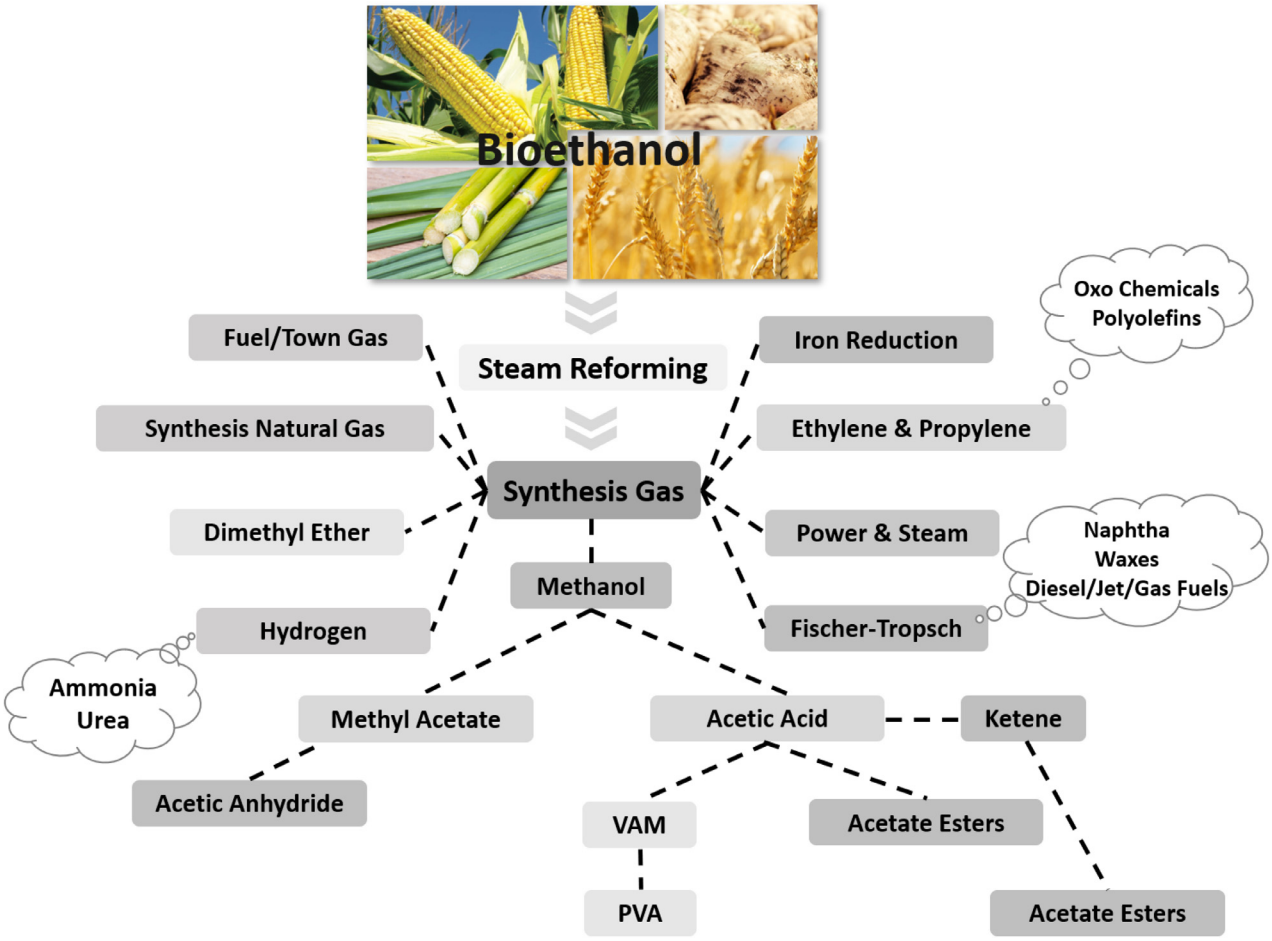


**Fig. 2.** Flow diagram for the production of fuels/chemicals *via* synthesis gas from ESR.

example, the catalytic upgrading of bioethanol to butanol (and ethanol to butanol [2,31]) has been reviewed [32,33]. The effect of bioethanol impurities on steam reforming for hydrogen production was studied by Sanchez et al. [34]. However, those reviews on the catalytic conversion of bioethanol mainly focus on a single product. Herein, we aim to provide a comprehensive review of catalytic conversion of bioethanol to a variety of chemicals and fuels including hydrogen, $C_2$–$C_4$ olefins, and gasoline. Specifically, we focus on the relationships between the catalyst, reaction mechanism and the catalytic activity and stability. Bioethanol conversion to other small oxygenates such as acetaldehyde, diethyl ether, acetic acid, acetone, and ethyl acetate is also covered. Finally, a brief discussion of the future research into the improved catalyst design for various conversions is also provided. It should be noted that (i) both petrochemical ethanol and bioethanol have the identical chemical formula but produced from different origins, and (ii) ethanol is mostly produced *via* fermentation, *i.e.* bioethanol, since the 1980s. Therefore, in this review, we do not distinguish the specific meaning of "ethanol" and "bioethanol", *i.e.*, all represent sustainable ethanol derived from biomass.

## 2. Bioethanol to hydrogen

Ethanol steam reforming (ESR) of is an attractive method for producing $H_2$ and synthesis gas (syngas, a mixture of $H_2$ and CO) [35]. Hydrogen is a clean energy source which is regarded as a feasible replacement for fossil fuels [36]. Besides, it can be used for ammonia production, petroleum refining (*e.g.*, hydrocracking), welding, and fuel cells. Syngas can either be used directly as fuel or as a platform feedstock to produce various fuels/chemicals such as diesel, methanol, and dimethyl ether *via* catalytic routes, as shown in Fig. 2 [37]. The use of bioethanol as a feedstock for the production of $H_2$ has many advantages including (i) independent from fossil fuels, (ii) abundant and sustainable source and (iii) reduction in the net amount of greenhouse gas emissions [29,38,39].

### 2.1. Catalytic reaction mechanism of ESR

Stoichiometrically, the overall reaction of ESR is shown in Eq. (1) [37,40], *i.e.*, ethanol reacts with water steam to give carbon dioxide ($CO_2$) and hydrogen ($H_2$). ESR is an endothermic process ($\Delta H$ = +173.3 kJ/mol) and therefore high reaction temperatures (300–800 °C) are necessary [41]. It was found that the use of steam/ethanol (S/E) molar ratio in the feed above the stoichiometric value (S/E = 3) improves the selectivity to $H_2$ [42]. More importantly, the use of high S/E ratios (>10) in ESR may allow the use of crude bioethanol directly as the feedstock without the need of separating water from ethanol via distillation.

$$CH_3CH_2OH + 3H_2O \leftrightarrow 2CO_2 + 6H_2 \quad (1)$$

As shown in Fig. 3, the reaction mechanism is rather complex since different parallel reactions (Eqs. 2–15) occur simultaneously along with $H_2$ production, such as dehydration into ethylene (Eq. 12), dehydrogenation into acetaldehyde (Eq. 3), condensation to acetone (Eq. 6), and decomposition reaction (Eq. 2). Gursahani et al. suggested that the first step of the system is the dissociative adsorption of ethanol to form ethoxy species, which undergo dehydrogenation to generate acetaldehyde and acetyl intermediates [43]. These species can further decompose *via* C-C bond cleavage to produce CO, $CH_4$, and $H_2$. Temperature programmed desorption (TPD) experiments have shown that acetone

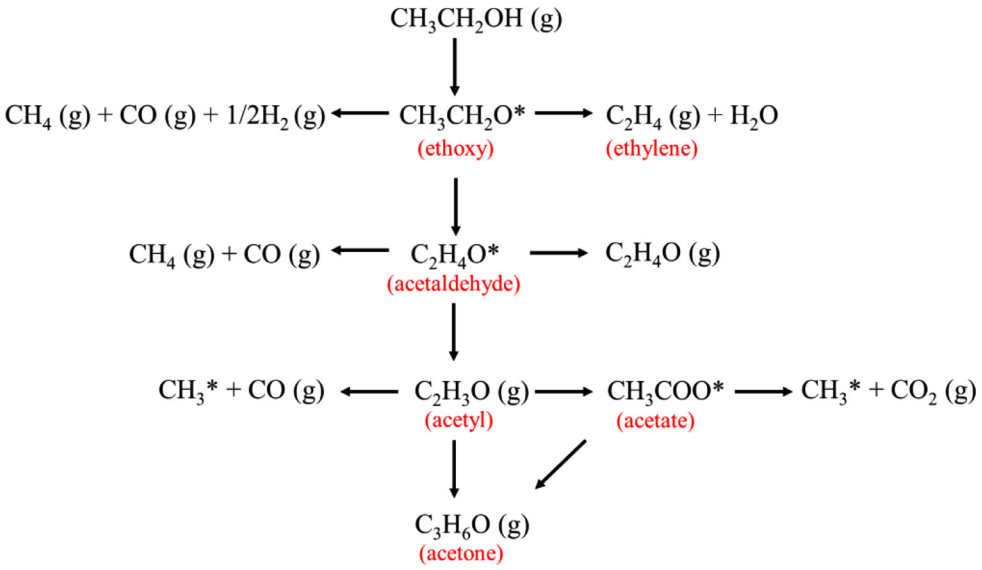


**Fig. 3.** Possible reaction pathways of ESR [41,45,46].

and ethylene were produced during ethanol desorption. Acetone formation can occur from two possible pathways, that is, (i) coupling of two acetate molecules and (ii) disproportionation of two acetyl species. Ethylene can be formed *via* ethanol dehydration, depending on the acid/base properties of the support [35,41,44]. Ethylene can further polymerise or cyclise to form coke on the catalyst, deactivating the catalyst.

The relative contribution of different reactions (to the production distribution) during ESR depends on both the nature of the catalyst (including the active sites and the support) and the reaction conditions used, *e.g.*, temperature, feed composition (or water/ethanol ratio), and residence time (or feed flow rate). The effect of the operating parameters on the efficiency of ESR has been extensively discussed previously [41,42,45]. Hence, catalysts that were exclusively developed for ESR are critically reviewed here with relevant discussion on catalyst deactivation during ESR.

Ethanol decomposition:

$$CH_3CH_2OH \leftrightarrow CH_4 + CO + H_2 \quad (2)$$

Ethanol dehydrogenation:

$$CH_3CH_2OH \leftrightarrow CH_3CHO + H_2 \quad (3)$$

Acetaldehyde decomposition:

$$CH_3CHO \leftrightarrow CH_4 + CO \quad (4)$$

Acetaldehyde steam reforming:

$$CH_3CHO + H_2O \leftrightarrow CH_4 + CO_2 + H_2 \quad (5)$$

Acetone formation:

$$2CH_3CH_2OH \leftrightarrow CH_3COCH_3 + CO + 3H_2 \quad (6)$$

Acetone steam reforming:

$$CH_3COCH_3 + 3H_2O \leftrightarrow 3CO + 6H_2 \quad (7)$$

Methane steam reforming:

$$CH_4 + 2H_2O \leftrightarrow CO_2 + 4H_2 \quad (8)$$

Water gas shift (WGS):

$$CO + H_2O \leftrightarrow CO_2 + H_2 \quad (9)$$

Methanation:

$$CO + 3H_2 \leftrightarrow CH_4 + H_2O \quad (10)$$

$$CO_2 + 4H_2 \leftrightarrow CH_4 + 2H_2O \quad (11)$$

Ethanol dehydration:

$$CH_3CH_2OH \leftrightarrow CH_2CH_2 + H_2O \quad (12)$$

Ethylene decomposition:

$$CH_2CH_2 \leftrightarrow 2C + H_2 \quad (13)$$

Methane decomposition:

$$CH_4 \leftrightarrow C + 2H_2 \quad (14)$$

Boudouard reaction:

$$2CO \leftrightarrow CO_2 + C \quad (15)$$

### 2.2. Catalysts for ESR

Supported metal catalysts are commonly used for efficient ESR. Typically, metallic phases are responsible for cracking both C-C and C-H bonds of hydrocarbons, whilst the support is commonly responsible for activating the steam to generate highly mobile oxygen, which can diffuse onto metals to stabilise the metal particles and facilitate steam gasification of coke. Various catalysts have been extensively studied in ESR, including both noble metals and transition metals [37,45,47].

#### 2.2.1. Noble metal catalysts

Liguras *et al.* studied the catalytic activity of noble Pt, Pd, Rh, and Ru metals supported on $Al_2O_3$ catalysts in ESR [48]. Rh catalyst presented the best activity with high hydrogen production ability due to its high activity for C-C and C-H bond dissociations, which were necessary for ethanol conversion [49]. $Rh/CeO_2$ catalyst showed good selectivity to $H_2$ and suppressed coke deposition, enhancing long-term stability in ESR due to the oxygen storage-release capability of $CeO_2$ support [50]. Similarly, $La_2O_3$ was also confirmed to be the excellent support or promoter to increase metal-support interaction, metal dispersion, and

anti-coking capability [51]. The stability of $Rh/Al_2O_3$ catalyst was significantly improved by adding $La_2O_3$ and $CeO_2$ [52]. $La_2O_3$-$CeO_2$ with the combined effect of the formation of lanthanum oxycarbonate and high mobile lattice oxygen was beneficial to enhance carbon gasification reaction, avoiding carbon deposition.

Pt catalysts are highly active in ESR with high selectivity towards hydrogen. Basagiannis et al. compared the catalytic performance of various metal supported on $Al_2O_3$ catalysts and established the activity order of Pt > Pd > Rh > Ru [53]. It was found that Pt improved ethanol decomposition and dehydrogenation reactions and the $Al_2O_3$ support interacted strongly with ethanol molecules, promoting the dehydration reaction to form $C_2H_4$. Pt catalysts loaded on different supports such as $ZrO_2$, $TiO_2$, $CeO_2$, and activated carbon (AC) have also been investigated [54]. The activity based on the measured conversions varied in the order of $Pt/CeO_2$ > $Pt/ZrO_2$ > $Pt/TiO_2$ ≈ Pt/AC. The comparatively high activity of $Pt/CeO_2$ was due to the good $O_2$ storage-release capability of the $CeO_2$ support, which could suppress carbon deposition and increase $H_2$ production simultaneously [55].

Neutralising acid sites by adding basic promoters has been demonstrated to be an effective approach to prevent coke formation by promoting the gasification reaction [56,57]. For example, Na doping of $Pt/ZrO_2$ benefited the selectivity to $H_2$ [58]. It was suggested that in the presence of Na promoter, acetate decarboxylation pathway was favoured, while the decarbonylation pathway was preferred over the pristine $Pt/ZrO_2$. The latter pathway tends to reduce the $H_2$ selectivity of the overall process. Additionally, alloying Pt with a second metal (*e.g.* Cu [59] or Sn [56]) could also enhance the performance of the resulting catalysts in ESR.

Since supported metal nanoparticle catalysts (dispersed on oxide supports) are prone to agglomerate during catalysis, resulting in the reduced active catalytic sites and catalyst deactivation, structured core-shell catalysts (such as encapsulated Pt nanoparticles within porous materials) have been developed to address the issues. Encapsulation strategy can prevent the aggregation of Pt nanoparticles, as well as suppressing the coke formation on the active metal surface. Dai et al. synthesised dragon fruit-like Pt-Cu@m$SiO_2$ catalyst (Pt-Cu as the core and $SiO_2$ as the shell), which showed excellent performance regarding both activity and stability for low-temperature ESR at 250–450 °C [60]. Sun et al. developed the Pt-$CeO_2$@Ni-$SiO_2$ catalyst with yolk-shell structures for increasing hydrogen production from ESR, and the catalyst yielded high $H_2$ selectivity (~67%) at 400 °C [61].

Supported Ru catalyst has also been developed for steam forming due to its ability to cleave the C-C bond and cost-effectiveness as compared with Rh and Pt catalysts. Different oxide supports (of $Al_2O_3$, $CeO_2$, $TiO_2$, and $SiO_2$) were used to prepare supported Ru catalysts for a comparative study in ESR [62]. Among them, the $Ru/CeO_2$ catalyst showed the comparatively best performance because $CeO_2$ was active support for the redox process in reforming processes, increasing the rate of oxidation reaction and reducing the deposition of intermediates on metal surface [63]. Additionally, preparation of Ru catalysts with small metal particles is a good strategy to achieve high catalytic activity at low metal loadings [64].

Pd catalyst has also shown good performance for $H_2$ production with insignificant CO formation at low temperatures (300–500 °C). Barrios et al. [65] studied methanol steam reforming over $Pd/CeO_2$ and $Pd/ZnO/CeO_2$ catalysts and found that the steam reforming reaction occurred only in the presence of ZnO. $Pd_{0.01}Zn_{0.29}Mg_{0.7}Al_2O_4$ catalyst was developed for ESR, which achieved 80% yield of $H_2$ and 100% ethanol conversion, as well as showing an excellent catalytic stability, *i.e.*, being stable for 30 h at 450 °C [66].

### 2.2.2. Transition metal catalysts

Although noble metal catalysts have high activity and stability in SR, the resource scarcity and relatively high costs of these catalysts can be the obstacle for their applications at large scales. Transition metal-based catalysts, especially Ni and/or Co-based catalysts [67–69] are frequently used in industry for SR due to their relatively low cost and good activity for C-C and C-H bond cleavage. $Al_2O_3$-supported Ni, Co, Fe, and Cu catalysts were evaluated for steam reforming [70]. The results showed that the reaction rate over the Fe and Cu catalysts was significantly lower than that over the Ni and Co catalysts. In comparison with monometallic Ni catalyst, bimetallic Ni-Co catalyst showed the enhanced coke resistance ability, and thus improved the stability [71]. You et al. found the addition of Co to $Ni/Al_2O_3$ decreased metal particle size, and improved metal dispersion and metal-support interaction, which effectively enhanced the stability of catalyst by suppressing carbon deposition, being beneficial to CO hydrogenation, methane partial oxidation, and steam reforming reactions [72]. Bimetallic Ni-Co catalyst supported on $Al_2O_3$-MgO exhibited excellent stability without significant deactivation even after 2000 h on stream [73]. In addition to Co, other metals (*e.g.* Mg [74], Ca [75], Cu [76], La [77], and Ce [78]) were also used as the promoter in the Ni-based catalysts for improving steam reforming reactions.

Due to the acidic nature of $Al_2O_3$, formation of ethylene, a precursor of coke, can be favoured. Therefore, alkali metal doping was proposed to modify the acidity of $Al_2O_3$ to improve catalyst stability [35,37,40]. For example, a Ni supported on spinel $MgAl_2O_4$ catalyst exhibited better performance regarding $H_2$ productivity and catalyst stability than the catalyst supported on $Al_2O_3$ [79]. In comparison with the pristine $Al_2O_3$, the reduced acidity of $MgAl_2O_4$ suppressed coke formation from ethylene polymerisation. Mg-Al hydrotalcites are also promising candidate supports for preparing supported Ni catalysts due to its high surface area and thermal stability, as well as the controllable acid/base properties. The presence of Mg in the support can enhance catalyst stability, while low Al content helps to increase catalytic activity to improve $H_2$ production. Incorporation of Ni metals into the hydrotalcite matrix creates highly dispersed metal oxides and gives excellent results in both activity and stability. Additionally, hydrotalcite-derived materials can act as $CO_2$ adsorbent during steam reforming [80–83], making it to be a promising material to achieve simultaneous reaction and separation of $CO_2$ for the production of pure $H_2$ in a single step.

Silica materials, especially mesoporous silica with the ordered structure and uniform pore size distribution, are good supports for preparing Ni catalysts for ESR [40,84]. SBA-15 [85–88], MCM-41 [89,90], and KIT-6 [91,92] are the most commonly used mesoporous silica supports to enhance the Ni dispersion, and hence the catalytic activity and stability. However, large Ni nanoparticles on the external surface of silica have weak interaction with the support at elevated temperatures, causing catalyst deactivation easily. Development of bimetallic catalyst has been proved to be a good strategy to overcome the deactivation problem, and also to improve the catalyst activity. The addition of other metal promoters (*e.g.* Rh, Pd, Cu, Ce, Co, Au, and Mo) to Ni catalysts could improve its anti-sintering capacity [41,45,85,93]. As compared with the monometallic Ni/MCM-41 and Co/MCM-41 catalysts, the bimetallic Co-Ni/MCM-41 catalyst showed the best catalytic performance (with about 90% ethanol conversion and 80% $H_2$ yield) [89]. The good activity and stability of the developed bimetallic catalyst were due to the improved Ni dispersion on the support and the strengthened metal-support interaction [87]. Finally, it is worth mentioning that the catalyst preparation method and the selection of metal precursors also play an important role in tuning the metal-support interaction and catalyst performance in SR [88,94,95].

The application of carbon-based materials as the catalyst supports has been extensively studied in steam reforming processes [30,96-98]. Cao et al. [99] found that Ni/AC showed higher coke resistance than $Ni/Al_2O_3$. The addition of different metal oxides (*i.e.*, MgO, $La_2O_3$, and $Y_2O_3$) to Rh/AC was effective to increase $H_2$ yield [96]. Carbon-supported bimetallic CoRu [100], and trimetallic Ni/Cu/Pd [97] catalysts were also reported for ESR. Additionally, carbon nanomaterials such as carbon nanofibers [101], carbon nanotubes [102–104], and graphene [105] have attracted considerable attention as the catalyst supports due to their capability of enhancing metal dispersion with small

metal particles. In addition, the high $\pi$-electron density of carbon nanomaterials is beneficial to promote electron transfer between the metal and support, thus improving the catalytic performance.

Catalysts derived from perovskites (*e.g.*, $LaNiO_3$) also show the potential for ESR due to their high oxygen mobility, which has the advantage in removing coke deposition [106–108]. It was found that in the $La_{1-x}Ce_xNiO_3$ perovskite-type oxides (*via* partial substitution of La by Ce), an increase in oxygen vacancies could reduce the size of Ni particles within, which could inhibit carbon accumulation during ESR [109,110]. Sekine et al. studied the effect of the partial replacement of La by Sr in $Ni/LaAlO_3$ for steam reforming of toluene. They found an increase in lattice oxygen mobility in the Sr-substituted catalyst, which enhanced its catalytic activity and suppressed carbon deposition [111]. In addition, substitution of Ni by Co in perovskite $LaNiO_3$ exhibited excellent resistance to sintering at 700 °C [112,113], and Ni substitution by Fe showed improved activity, selectivity and stability in steam reforming reactions [114–116].

In additions to Ni catalysts, Co catalysts are also effective for cleaving C-C bond, especially at temperatures above 400 °C, showing good selectivity to $H_2$ and $CO_2$. $Co/Al_2O_3$ showed lower activity as compared with $Co/SiO_2$ due to the strong interaction between Co metal and $Al_2O_3$, which made it difficult to be reduced [117]. Song et al. studied the effect of catalyst supports on the performance of the supported Co catalysts in ESR [118]. The findings established the order of activity and stability as $Co/Al_2O_3 < Co/ZrO_2 < Co/CeO_2$, which was probably related to the surface acidity and oxygen mobility. Supported Co catalysts based on other supports (*e.g.* zeolite [119] and hydrotalcite [120]) were developed and explored as well for steam reforming processes.

### 2.3. SR of crude bioethanol

Crude bioethanol is usually a mixture of water and ethanol with other organic impurities, such as aldehydes, amines, acids, and esters, from fermentation processes. Therefore, purification may be necessary to remove these impurities to avoid catalyst deactivation during ESR. However, purification of bioethanol is always energy intensive, and hence SR of crude bioethanol is a cost-effective strategy for $H_2$ production [121,122].

The $Ni/Al_2O_3$ catalysts prepared by precipitation methods possessed smaller Ni particles and showed higher activity in SR of bioethanol as compared with that prepared by co-precipitation and impregnation methods [123]. Mondal et al. investigated catalytic oxidative and non-oxidative bioethanol steam reforming in a tubular fixed-bed reaction system using 30 wt.%$Ni/CeO_2$-$ZrO_2$ and 1 wt.%Rh-30 wt.%$Ni/CeO_2$-$ZrO_2$ [121]. Oxidative steam reforming decreased both $H_2$ yield and selectivity due to the partial oxidation of oxygenates compounds present in the feedstock. Comparatively, Rh-containing catalyst showed higher catalytic stability. Dan et al. studied steam reforming of bioethanol produced from wood waste in the presence of $Ni/Al_2O_3$ catalysts [124]. The results showed that the addition of $La_2O_3$ and $CeO_2$ to the $Ni/Al_2O_3$ catalyst exhibited higher activity and stability with respect to the pristine $Ni/Al_2O_3$ catalyst. However, the acetic acid conversion (one of the impurities in crude bioethanol) was only approximately 30%. Among all catalysts studied, $Ni/La_2O_3$-$Al_2O_3$ showed the highest $H_2$ production activity and remained stable for 4 h time on steam at 350 °C.

Valant et al. studied the effect of various organic impurities on SR of bioethanol over the $Rh/MgAl_2O_4$ catalyst [125]. Adding butanal or diethylamine into the feedstock increased ethanol conversion without changing the product selectivity. In contrast, in the presence of other organic compounds, such as butanol, ethylether, and ethyl acetate, ethanol conversion decreased, and apparent deactivation of the catalyst was observed due to carbon deposition. Moreover, selectivity to $H_2$ decreased significantly, while an increase in intermediate products, especially ethylene, was measured. SR of crude bioethanol containing 1 mol% of other alcohol impurities over 1%$Rh/MgAl_2O_4/Al_2O_3$ was also investigated [126]. It was found that alcohol impurities in the crude bioethanol played an important role in improving $H_2$ production during the catalysis. The results showed that 1 mol% of methanol in bioethanol slightly increased the hydrogen yield without affecting ethanol conversion. Conversely, the presence of higher alcohols decreased both ethanol conversion and hydrogen yield during ESR due to catalyst deactivation. It was also found that catalyst deactivation increased with an increase in carbon atom numbers of the alcohols, and it became more pronounced with brunched alcohols compared to linear ones. In addition, Sanchez et al. reviewed the effect of impurities in bioethanol (including alcohols, amines, aldehydes, ketones, and sulfur components) on ESR [34]. It was found that impurities such as fusel alcohols and acetic acid contributed to coking significantly, whilst other impurities such as methanol and aldehydes enhanced $H_2$ yield due to the relatively high reactivity under the ESR conditions.

### 2.4. Catalyst deactivation

Catalyst deactivation is one of the main problems of ESR, which are commonly due to carbon deposition and metal sintering [41,127,128]. Carbon deposition on the catalyst causes pore blockage and then limits the accessibility of active sites to reactant molecules, resulting in lower conversions and lower yield and selectivity towards the target product, and the reduced catalyst life. Regarding metal sintering, it is caused by the agglomeration of small metal particles under thermal conditions during the reaction. As a result, it causes the loss in the active metal surface area, and thus reduces the catalyst activity.

#### 2.4.1. Carbon deposition

Several reactions may contribute to carbon deposition on the catalyst used in ESR: (i) ethanol dehydration to ethylene which can polymerise to coke Eq. (16)), (ii) acetone aldol condensation (Eq. 17), (iii) Boudouard reaction (Eq. 15), (iv) reverse carbon gasification (Eq. 18), and (v) methane and ethylene decomposition (Eqs. 19 and (20) [41]. Generally, carbon deposition depends on the reaction conditions (such as temperature and water/ethanol molar ratio) and the catalyst used. The Boudouard reaction and reverse carbon gasification are favoured at low reaction temperatures, whereas higher temperatures favour the carbon formation *via* the decomposition of hydrocarbons. Carbon deposition over metal catalyst has been extensively studied [129,130].

Ethylene polymerization:

$$CH_2CH_2 \rightarrow \text{coke} \quad (16)$$

Acetone aldol condensation:

$$2CH_3COCH_3 \rightarrow (CH_3)_2C(OH)CH_2COCH_3 \quad (17)$$

$$\rightarrow (CH_3)_2C = CHCOCH_3 + H_2O$$

Reverse carbon gasification:

$$CO + H_2 \leftrightarrow C + H_2O \quad (18)$$

Methane decomposition:

$$CH_4 \leftrightarrow C + 2H_2 \quad (19)$$

Ethene decomposition:

$$CH_2CH_2 \leftrightarrow 2C + 2H_2 \quad (20)$$

As shown in Fig. 4, there are three different types of carbonaceous materials (amorphous, filamentous, and encapsulating carbon) formed on Ni catalyst during steam reforming [131,132]. Amorphous carbon formed at low temperatures between 200–500 °C, whilst the formation of filamentous carbon was favoured at higher temperatures [133]. The

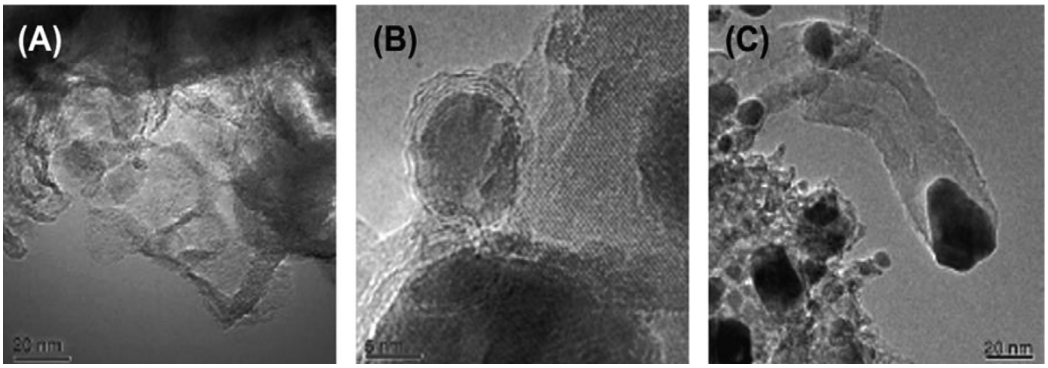


**Fig. 4.** TEM images of different types of carbon formed over a Ni/$MgAl_2O_4$ catalyst (A) amorphous, (B) encapsulating, and (C) filamentous carbon. Reprinted with permission from ref [131]. Copyright (2006) Elsevier.

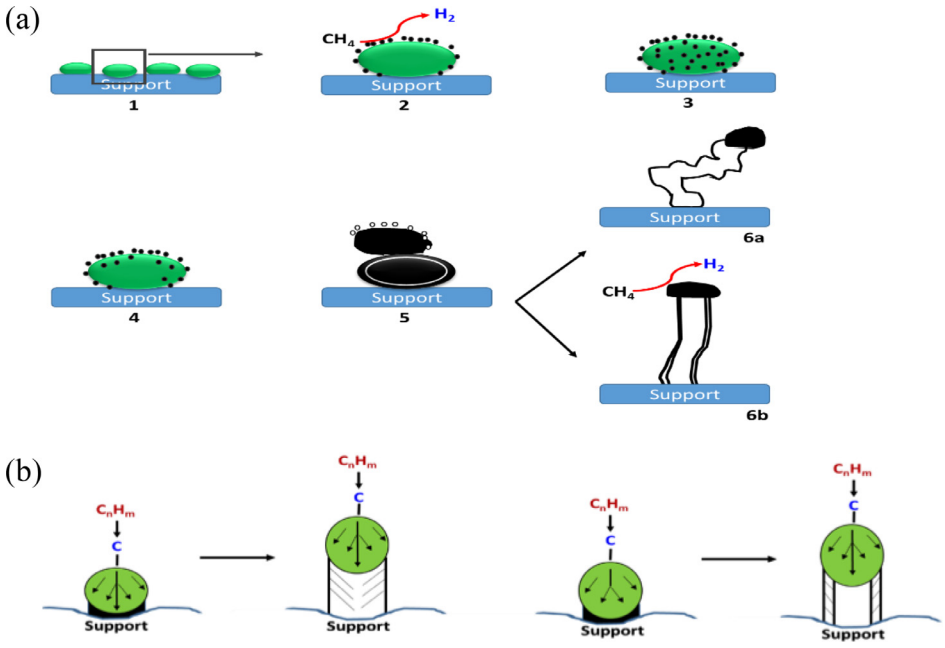


**Fig. 5.** (a) The mechanism for the formation of CNTs and CNFs over a supported catalyst (b) the formation of CNFs (left) and CNTs (right) [135].

growth of filamentous carbon was believed to occur when carbon species diffused into the Ni particles and formed nickel carbide (Ni-C). Ni-C was metastable active carbide between nickel metal and graphite, which formed the encapsulated Ni particles [134]. Carbon deposition continued on the surface of nickel until the carbon content was high enough to push Ni off from the surface of the support to form carbon nanotubes (CNTs) and/or carbon nanofibres (CNFs), as shown in Fig. 5, and the formation of CNFs/CNTs was simultaneous during reforming process. For CNFs, the nucleation occurred across the entire metal-support interface through diffusion, resulting in the formation of full fibres (Fig. 5b). CNFs formation was generally facilitated at low temperatures when the nucleation rate was slow, and carbon atoms could reach the whole metal-support interface. The nucleation of CNTs was restricted to the vicinity of the gas-metal interface. The growth of CNTs might be favoured at high temperatures due to the high nucleation rate, *i.e.*, high nucleation rate enabled the formation of hollow fibres before carbon atoms arrived at the metal-support interface [135]. The formation of encapsulating carbon around a metal catalyst is initiated through the deposition of graphitic layers on the entire surface of the metal particle, as shown by the schematic mechanism in Fig. 6. The encapsulating carbon can cause catalyst deactivation, whilst in the case of the formation of filamentous carbon, in which the metal catalyst remains at the top of the filament and is accessible to reactants and intermediates, and the catalyst can maintain its activity during reforming reaction [136].

To date, many strategies have been proposed to minimise carbon deposition on catalysts during ESR, such as increasing water/ethanol ratio, co-feeding of $H_2$ and $CO_2$, and catalyst modification [137]. However, an increase in water/ethanol ratio requires higher temperatures to facilitate the reaction. Co-feeding of $H_2$ enables hydrogenation of the deposited carbon to mitigate deactivation, but it also increases the yield of hydrocarbons. The addition of $CO_2$ competes with ethanol adsorption on active sites, though it reduces carbon deposition. Therefore, catalyst modification may be the rational choice for minimising deactivation due to coking. Relevant research has shown that active metals (and promoters), catalyst supports, and the synergistic interactions between metals and supports can be optimised to suppress coke formation during ESR [30,41,137].

### 2.4.2. *Metal sintering*

Metal sintering causes the loss in the active metal surface area due to the agglomeration of small metal particles into larger ones [129]. Sintering is also affected by many factors, such as reaction temperature, gas composition over the catalyst, structure and composition of the catalyst, and the catalyst support and metal-support interactions. Among them, reaction temperature may be the primary reason for causing metal sintering [41,127]. It was found that an increase in the reaction temperature accelerates the sintering process [127]. To avoid metal sintering during catalysis, suitable catalyst preparation methods should be used

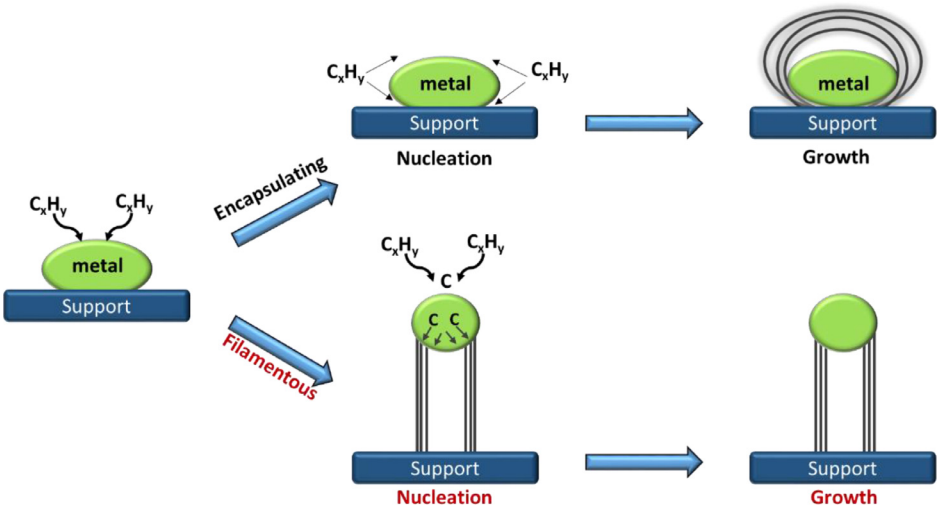


**Fig. 6.** Schematic presentation of the growth mechanism of encapsulating and filamentous carbon due to carbon deposition in reforming systems [136].

to allow the formation of metal particles with small sizes and high dispersion, which can activate ESR under mild conditions (*e.g.*, at low reaction temperatures of 300–600 °C and 1 atm) [138–140]. For example, Ni/MMT-$TiO_2$ nanocomposite catalyst (Ni/$TiO_2$ nanoparticles dispersed on montmorillonite clay, MMT) showed enhanced Ni-dispersion and reducibility and achieved an ethanol conversion of 89% and a $H_2$ yield of up to 55% at 500 °C and 1 atm [139]. Hydrogen yield over Ni/MMT-$TiO_2$ nanocomposite was 1.5-fold more than that obtained over the catalyst with microparticles. Besides, the nanostructured Ni/MMT-$TiO_2$ catalyst exhibited better stability compared to the catalyst with microparticles. Cobalt-based nanoparticles have also been demonstrated as active catalysts for low temperature (~500 °C) $H_2$ production by ethanol steam reforming [138]. Additionally, the engineering of support-metal configuration/interaction is also important to enable the segregation of metal nanoparticles or strong interaction between the two to stabilise the catalyst particles [127]. Palma et al. found that catalyst deposition on high surface area silica improved metal dispersion and metal-support interaction, which prevent metal sintering and coking to a large extent compared to that on the silica-free sample [140].

## 3. Bioethanol to $C_2$–$C_4$ olefins

$C_2$–$C_4$ olefins are important platform molecules for the production of a variety of chemicals. Due to the cost-effectiveness and eco-friendly nature of bioethanol, it has been explored for producing light olefins.

### 3.1. Bioethanol to ethylene

Ethylene, as an important feedstock in petrochemical industry, is mainly used in the production of polyethylene (one of the most common plastics used in our daily life, and primarily used for packaging, *i.e.* plastic bags, films, and bottles), ethylene oxide (used for producing chemicals and intermediates, such as ethylene glycol, glycol ethers, and ethoxylates), ethylene glycol (as a raw material in the manufacture of polyester fibres and for antifreeze formulations), and polyvinyl chloride (also a type of plastic polymer, and commonly used for producing pipes and as the insulation on electrical cables) [141]. At present, the climbing price of ethylene (from 697 US dollars per metric ton in 2020 to 1,014 US dollars per metric ton in 2021 [142]) and the sustainable features of bioethanol make the route of bioethanol to ethylene attractive [143–145].

#### 3.1.1. Catalytic reaction mechanism of ethanol-to-ethylene (ETE)

Fig. 7 shows a typical overview of ethanol-to-ethylene reaction network including the electron transfer steps. Path A is the concerted (direct) mechanism of ethanol dehydration to ethylene. Path B and Path C show the stepwise (indirect) dehydration mechanism [145,146], that is, the transformation of ethanol to diethyl ether (DEE, reaction intermediate), followed by the conversion of diethyl ether to ethylene. Path A is endothermic, in which a closed system usually adsorbs thermal energy from its surroundings, that is, heat transfer into the system. Conversely, the reaction of path B is exothermic, *i.e.*, releasing heat during reaction (the overall standard enthalpy change, $\Delta H$, is negative). Therefore, at relatively high temperatures, path A is preferred, while path B dominates the reaction at low temperatures. It was found that co-existence of the concerted and stepwise reaction pathways is common during the reaction [147], and both pathways can be inhibited by the presence of water [148]. In the system, ethylene may undergo subsequent reactions, such as oligomerisation, cyclisation, and aromatisation, to generate higher hydrocarbons, being responsible for forming coke deposits [146].

*3.1.1.1. Path A: Concerted reaction mechanism.* As shown in Fig. 8, E1 (single-molecule elimination reaction), E1cB (single-molecule conjugate base elimination reaction), and E2 (bimolecular elimination reaction) mechanisms have been proposed for direct ethanol dehydration to ethylene (path A), depending on catalysts and reaction conditions used [10]. E1 mechanism is normally found on acidic catalysts. Carbocation intermediate and water are formed by the protonation of alcoholic oxygen and the cleavage of the intramolecular C-O bond. The adjacent carbon then deprotonated on the basic sites to form unsaturated alkene product. Conversely, the E1cB mechanism proceeds over basic catalysts, in which C-H bond cleavage occurs first, forming carbanion or alkoxy intermediate, and then hydroxyl group on the alcohol carbon is eliminated on the acid sites to produce alkene. Both E1 and E1cB reaction pathways include the formation of ionic intermediates, while in E2 mechanism, the elimination of hydroxyl group on acid and the proton on base occur simultaneously by breaking C-O and C-H bonds to form alkene without intermediates. According to the substitution reaction grade rules of primary alcohols like ethanol, it is difficult to form stable carbocation intermediates due to the high-energy barrier. Therefore, direct dehydration of ethanol to ethylene mainly follows the E2 mechanism.

*3.1.1.2. Paths B and C: Stepwise reaction mechanism.* In the stepwise mechanism, two ethanol molecules form DEE *via* intermolecular dehydration (path B), which is then dehydrated to generate ethylene (path C). Zhang *et al.* summarised the mechanism of ethanol dehydration, and suggested an optimal reaction temperature range (under 240 °C) for DEE formation. When the temperature was above 240 °C, ethanol might convert directly to ethylene [149]. It is because that the reaction of path A is endothermic ($\Delta H$ = +44.9 kJ/mol) and an increase in reaction temper-

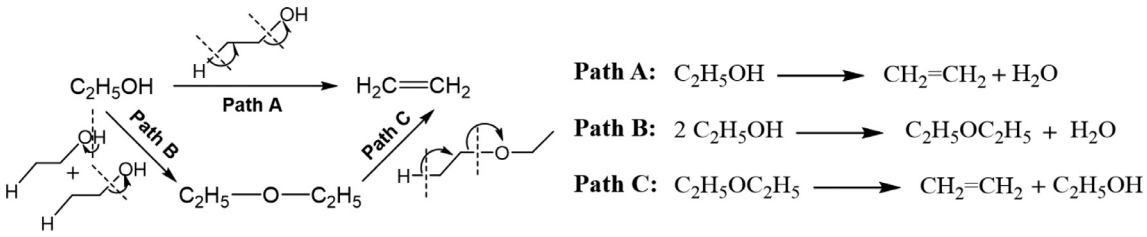


**Fig. 7.** Electron transfers in ETE reaction network.

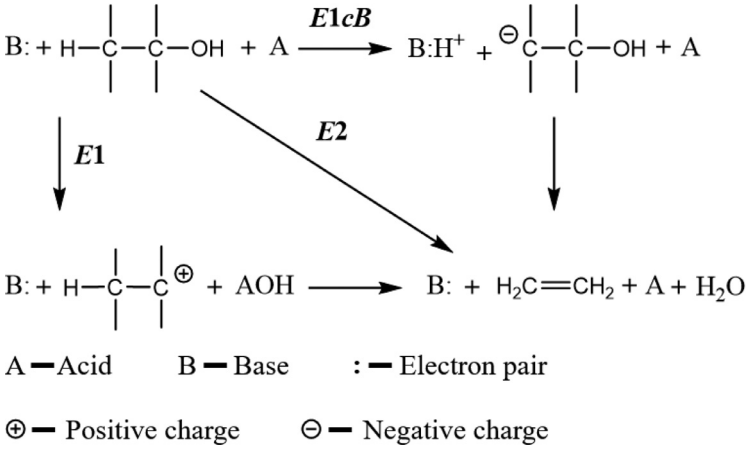


**Fig. 8.** Proposed reaction mechanism for alcohol dehydration [10,149].

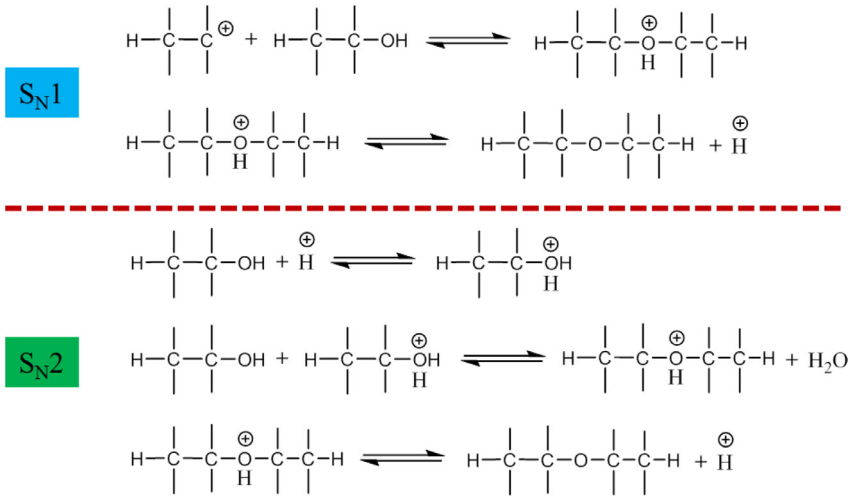


**Fig. 9.** Proposed reaction mechanism for the generation of diethyl ether from ethanol [149].

ature will shift the equilibrium to the right-hand side, and thus promote the reaction of path A. In contrast, the reaction of path B is exothermic ($\Delta H = -25.1$ kJ/mol), so a decrease in temperature favours path B. Although the consensus on the formation mechanism of DEE from ethanol has not yet been established, alkoxide (hydroxyl hydrogen of ethanol is replaced by a metal ion) is suggested as a necessary intermediate. The reaction of ethanol intermolecular dehydration to DEE is a substitution reaction, and the generation of DEE follows $S_N1$ (single-molecule nucleophilic substitution) or $S_N2$ (bimolecular nucleophilic substitution) mechanism (Fig. 9) [149]. The oxygen atom in DEE has an unshared electron pair, which can be considered as a weak alkali. When it absorbs on the acidic sites of the catalyst, oxygen onium salt is formed and the C-O bond becomes weak and then breaks to form ethylene.

### 3.1.2. Catalysts for ETE reaction

The first attempt on ethanol dehydration to produce ethylene in the laboratory scale was performed possibly in 1795 by mixing and heating ethanol and sulphuric acid [10,150], showing that the conversion was catalysed by acid catalyst, which rationalise the potential of solid acid catalysts. Phosphoric-based acid catalyst was the first catalyst used in the industrial equipment for ETE processes [149]. It was then developed by the British Imperial Chemical Industries (ICI) by loading phosphate on clay or coke [151,152]. Bedia et al. found that phosphoric acid impregnated carbon catalysts could achieve almost 100% ethylene selectivity in ETE [141]. However, phosphoric-based acid catalysts are easily deactivated by coke deposition, which hindered their further development [149]. Currently, there are mainly three types of heterogeneous catalysts used for ETE, *i.e.* metal oxides [153], zeolites [154], and heteropolyacid catalysts [155].

*3.1.2.1. Metal oxide catalysts.* Various metal oxide catalysts have been developed and used to convert ethanol to ethylene. $\gamma$-$Al_2O_3$ is a typical example [144,156,157], which exhibited better dehydration performance than $TiO_2$ and $ZrO_2$ [158]. A combination of *ab* initio theoretical

calculations and TPD experiments demonstrated that ethanol dehydration reaction occurred through an E2-elimination mechanism involving Lewis acid sites (metal centres) and surface O and/or OH groups of the metal oxides (*i.e.* ethanol transferred its $\beta$-hydrogens to surface O or OH groups from the presence of dissociated water on the oxide surface). It was found that the dehydration barriers decreased as the carbenium-ion stability increased and the barriers were consistently lower when involving the bridged O compared to that with the OH groups. The difference in energy barriers between the bridged O and the OH groups was small on $TiO_2$ and $ZrO_2$ but became more pronounced in the case or $\gamma$-$Al_2O_3$. Since the dehydration barriers on the cluster of $\gamma$-$Al_2O_3$ were smaller than those on $TiO_2$ and $ZrO_2$ (regardless of whether or not bridged O or the OH groups were involved), $\gamma$-$Al_2O_3$ was demonstrated to be a better catalyst for ethanol dehydration than either $TiO_2$ or $ZrO_2$ [158]. Banzaraktsaeva et al. found that ring-shaped $\gamma$-$Al_2O_3$ catalyst (acid-modified alumina prepared by centrifugal thermal activation of hydrargillite) showed relatively high ethanol conversion and ethylene yield (4–5% and 5–7% higher, respectively) as compared with the trilobe-shaped catalyst [159]. Their follow-up study showed that acid modification of ring-shaped catalyst could improve ethanol conversion from 74.5% to 84.1%, and ethylene selectivity from 55.4% to 70.6% at 370 °C [160]. Ceria-zirconia mixed oxide ($Ce_{0.8}Zr_{0.2}O_2$) was also developed for the conversion of ethanol to ethylene, which reached 100% ethanol conversion and selectivity for ethylene at low temperatures of 200–300 °C [161]. Tungsten oxide ($WO_{3-x}$) with abundant oxygen vacancy showed efficient activity for ethylene production from photocatalytic ethanol dehydration at ambient temperature and atmospheric pressure, achieving a remarkable ethylene generation rate of 16.9 mmol/(g·h) and 94.9% of ethylene selectivity [153]. Additionally, highly active $TiO_2$/$\gamma$-$Al_2O_3$ catalyst has been successfully applied for the catalytic dehydration of bioethanol to ethylene in a microchannel reactor, showing a high ethanol conversion of 99.96% and ethylene selectivity of 99.4% [162]. In general, $\gamma$-$Al_2O_3$ shows good catalytic activity (that is, production of high purity ethylene with high yield) and stability, as well as being cost-effective (due to the wide availability and the easy production process). However, when the concentration of ethanol feedstock is low (<12 wt.% [162]), high temperature (>400 °C [10]) and low space velocity (0.23–1.17 $h^{-1}$ weight hourly space velocity (WHSV) in a traditional fixed-bed reactor [162]) are required for ethanol dehydration over $\gamma$-$Al_2O_3$, being energy intensive. Therefore, zeolite catalysts are proposed and explored for advancing the conversion.

*3.1.2.2. Zeolite catalysts.* The commodity value of low-concentration ethanol (*e.g.,* residual liquid recovered from bio-fermentation) can be fully exploited using zeolite catalysts. ZSM-5 zeolite was effective catalyst for ETE even with low ethanol concentration (as low as 2 vol.%) in the feed and at temperatures as low as 170 °C due to the strong acidity and shape selectivity of ZSM-5 [163]. Zeolite acidity has a significant effect on catalytic performance regarding ethylene selectivity and catalyst stability [164]. The presence of a high concentration of strong acidic sites could promote the secondary reactions of ethylene (*i.e.*, oligmerisation, cracking and coking) to form long-chain hydrocarbons and even carbonaceous deposit on the catalyst [163,165]. Si/Al ratios of 35–55 were found to be able to provide high ethylene selectivity whilst maintaining high activity and stability [166]. It was found that the unique microporous framework of ZSM-5 played a major role in achieving high ethylene selectivity by blocking the formation of bulky oligomeric compounds, *i.e.,* shape selectivity [163]. Since the micropores of the zeolite can be easily blocked by bulky molecules, leading to catalyst deactivation, mesoporous zeolites have been developed to improve mass transfer during reaction. For example, Sheng *et al.* performed steaming of H-ZSM-5 zeolite to create mesoporous zeolite of HT500 (treated at 500 °C), and the HT500 exhibited excellent catalytic performance regarding both activity and stability (*i.e.*, ethanol conversion and ethylene selectivity were higher than 95% for 350 h on stream) [167]. Additionally, HT500 reduced coke deposition significantly (*i.e.*, 0.007 wt.%/h on spent HT500 *versus* 0.042 wt.%/h on spent H-ZSM-5). Deactivation of H-ZSM-5 can be attributed to the accumulation of coke deposition on the catalyst, which reduces the accessibility of reactants to the inner framework where active acid sites sit. Coke deposition over zeolites correlates with strong acidity, explaining quick deactivation the parent H-ZSM-5, which has concentrated strong acid sites, and its poor performance in ethanol conversion and ethylene selectivity. In contrast, the lower acidity and lower ratio of Brønsted acid to Lewis acid (B/L) of HT500 after steaming suppressed the coke deposition, resulting in the relief of the channel blockage. Additionally, the mesopores of HT500 could also enhance the diffusion of reactants and products, and thus mitigating coke formation. Lanthanum-phosphorous modified H-ZSM-5 zeolite showed excellent catalytic performance and coking resistance, especially 0.5%La-2%P/H-ZSM-5, achieving 100% ethanol conversion and 99.9% ethylene selectivity at 240–280 °C, which could be attributed to the tuned acid sites, pore structure and the synergistic interaction between the lanthanum and phosphorus [168]. Chen *et al.* developed Mn and Zn modified SAPO-11 and SAPO-34 zeolites, and found that the Mn-SAPO-34 catalyst showed the best ethanol conversion (~99.4%) and ethylene selectivity (~98.4%) at 340 °C due to its large surface area, affording more opportunities for reactants to contact and react [143]. Masih *et al.* compared the catalytic performance of Rho zeolite with ZSM-5 and three $\gamma$-$Al_2O_3$ catalysts [169]. RhO zeolite exhibited superior catalytic activity with an excellent ethylene selectivity of 99% at 250°C and 100% ethanol conversion, which was due to its medium-strong acidic properties.

*3.1.2.3. Heteropolyacid catalysts.* Several heteropolyacid catalysts (*e.g.* $K_xH_{3-x}PW_{12}O_{40}$ ($0 < x < 3$) [155], $Cu_{0.5x}H_{3-x}PMo_{12}O_{40}$ ($x$ = 1, 2 and 3) [170], $Ag_3PW_{12}O_{40}$ and $Ag_3PMo_{12}O_{40}$ [171], $H_3PW_{12}O_{40}$, and $H_4SiPW_{12}O_{40}$ [172]) have been studied for ethanol dehydration to ethylene. Gurgul *et al.* found that $Ag_3PW_{12}O_{40}$ had higher catalytic activity than $Ag_3PMo_{12}O_{40}$, but its activity strongly depended on the relative humidity of air [171]. For example, 2% of relative humidity of air atmosphere could cause the decomposition of about 40% of Keggin anion in AgPW structure and the removal of water hydrated lattice silver in the catalyst diminished the quantity of available protons, and thus decreased ethanol conversion. Clemente *et al.* synthesised HPW/CZ catalysts ($H_3PW_{12}O_{40}$ supported on $Ce_{0.8}Zr_{0.2}O_2$ mixed oxide) and found that the conversion of ethanol to ethylene increased with HPW loading on the support, and these catalysts also had the potential of achieving 100% ethanol conversion and approximately 100% ethylene selectivity [161]. Bokade et al. studied the catalytic dehydration of bioethanol using dodecatungestophosphoric acid (DTPA) supported on montmorillonite (K-10) catalysts, and found that 30% m/m DTPA/K-10 catalyst showed better activity with 74% ethanol conversion and 92% ethylene selectivity at 250 °C in comparison with other acid catalysts used [173]. Almohalla et al. compared three heteropolyacids (tungstophosphoric acid (TPA, $H_3O_{40}PW_{12}{\cdot}nH_2O$), silicotungstic acid (STA, $H_4O_{40}SiW_{12}{\cdot}nH_2O$) and phosphomolybdic acid (PMA, $H_3Mo_{12}O_{40}P{\cdot}nH_2O$)) supported on carbon materials (activated carbon and graphite) for ethylene production from bioethanol [174]. The results showed that TPA/AC and STA/AC catalysts exhibited the best performance, achieving activity values of 40 μmol/(g·s) and 100% ethylene selectivity after 2 h of reaction at 250 °C. Moreover, for all catalysts studied, no significant reduction in ethanol conversion was observed by the addition of water in the feed stream of bioethanol, and the ethylene selectivity was maintained without showing major changes, indicating both AC and graphite are promising supports for heteropolyacid catalysts.

### 3.2. Bioethanol to propylene

Propylene is another important platform light olefin, which is widely used for the production of polypropylene plastics (*e.g.*, films and packag-

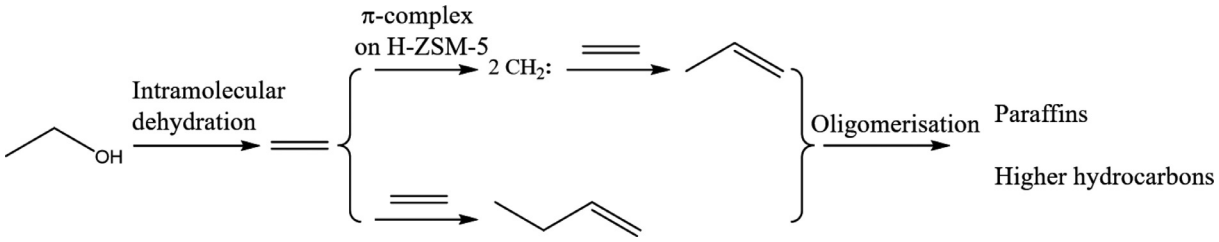


**Fig. 10.** Reaction pathways of ethanol conversion to propylene on H-ZSM-5 [177–179].

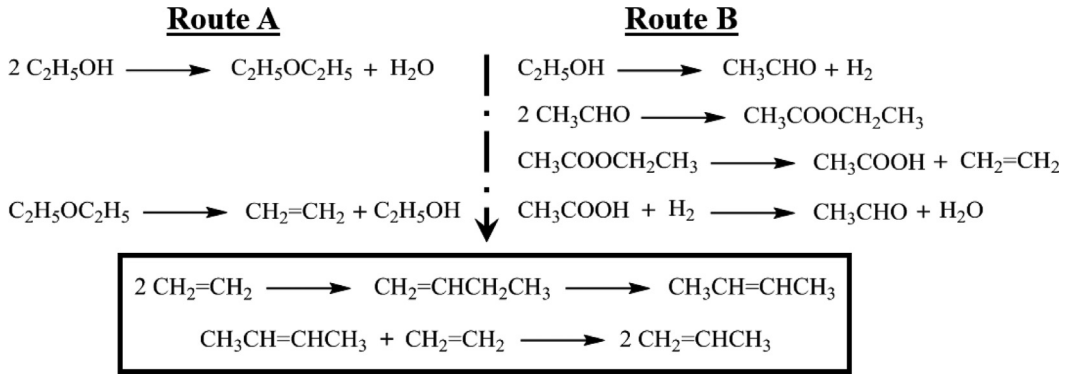


**Fig. 11.** Reaction pathways of ethanol conversion to propylene on Ni-MCM-41 [180].

ing), acrylonitrile (*e.g.*, polymer resins and synthetic rubbers) and propylene oxide (*e.g.*, polyether polyols used in flexible or rigid foams and propylene glycols used for food applications and in cosmetics) [20]. It is noted that propylene production growth rate has sustained at around 4% per year [175]. Although traditional technologies (the two main sources of propylene are as a by-product from steam cracking of liquid feedstocks such as naphtha and liquefied petroleum gas (LPG) from fossil fuels, and from off-gases produced in fluid catalytic cracking (FCC)) have been capable of meeting the demand so far, the feedstock fossil fuels are limited, non-renewable and unsustainable [175]. Therefore, it is urgent to develop new sustainable processes for propylene production. Since bioethanol can be produced from renewable biomass and is produced in a high capacity in the world, catalytic upgrading of bioethanol is now considered as a good alternative for propylene production [176].

### 3.2.1. Catalytic reaction mechanism of ethanol-to-propylene (ETP)

The reaction mechanism of ETP depends greatly on the catalysts employed. There are mainly three type of catalysts used for this process, *i.e.* zeolites [177–179], mesoporous materials [180], and metal oxides [180,181]. For H-ZSM-5 zeolite catalyst, as shown in Fig. 10, the proposed reaction mechanism includes ethanol dehydration to ethylene, which is then converted in parallel to propylene and butylene [179]. Finally, oligomerisation of ethylene, propylene and butylene contributes to the formation of paraffins and higher hydrocarbons. Iwamoto et al. identified two parallel pathways (route A and route B as shown in Fig. 11) of the propylene formation from ethanol over the Ni-MCM-41 catalyst [180]. Route A is a process that ethanol is firstly converted to diethyl ether by dehydration, which is then converted to ethylene, followed by the transformation of ethylene to butylenes (except isobutene), and then 2-butylene reacts with ethylene to produce propylene. For route B, instead of having diethyl ether as intermediate, acetaldehyde and ethyl acetate are observed as intermediates. Ethanol is firstly converted to acetaldehyde by dehydrogenation, which is then converted to ethyl acetate, followed by the formation of ethylene from ethyl acetate, and then ethylene is transformed to butylenes (except isobutene), and then 2-butylene reacts with ethylene to produce propylene (the conversion of ethylene to propylene in route B is the same as that in route A). For $Sc_2O_3/In_2O_3$ and $Y_2O_3/CeO_2$ catalysts [180], as shown in Fig. 12, the reaction includes dehydrogenation of ethanol to acetaldehyde, conversion of acetaldehyde to acetone, transformation of acetone to isopropanol, and dehydration of isopropanol to propylene. Although small quantities of ethylene and butylenes were found in the product, no propylene was obtained upon the introduction of ethylene into the reaction system, suggesting that metathesis reaction of ethylene and butylenes was unlikely to produce propylene. Fig. 12 only presents the principal reaction route found by Iwamoto et al. for the formation of acetone from acetaldehyde, and other reactions (*e.g.*, Eqs. 21–23) [180,181] may also occur simultaneously. Finally, it is worth noting that acetone is hydrogenated to form isopropanol over $Sc_2O_3/In_2O_3$, whilst, over the $Y_2O_3/CeO_2$ catalyst, acetone is reduced by ethanol instead of hydrogen, which is recognised as Meerwein-Ponndorf-Verley (MPV) reduction [180,182,183].

$$2\ CH_3CHO + H_2O \rightarrow CH_3COCH_3 + CO_2 + 2\ H_2 \quad (21)$$

$$CH_3COOCH_2CH_3 + H_2O \rightarrow CH_3COOH + C_2H_5OH \quad (22)$$

$$CH_3CHO + H_2O \rightarrow CH_3COOH + H_2 \quad (23)$$

Matheus et al. proposed another mechanism for ETP over a mixture of *t*-$ZrO_2$ and $AgCeO_2$ [175]. As shown in Fig. 13, the oxidative dehydrogenation of ethanol occurs first, forming acetaldehyde (over $AgCeO_2$), which is then oxidised to acetate species (over $AgCeO_2$). These acetate species undergo ketonisation to acetone (over $AgCeO_2$), which undergoes Meerwein-Ponndorf-Verley (MPV) reduction with ethanol to generate isopropanol and acetaldehyde (over *t*-$ZrO_2$). The former is dehydrated to propylene (over *t*-$ZrO_2$), while the latter goes back to oxidation and ketonisation (over $AgCeO_2$). Acetaldehyde can also be produced by the dehydrogenation of ethanol over *t*-$ZrO_2$.

### 3.2.2. Catalysts for ETP reaction

H-ZSM-5 zeolite is a typical catalyst used for the catalytic conversion of ethanol to propylene. One factor which affects the catalytic performance of H-ZSM-5 is its acidic property (which can be generally represented by the Si/Al ratio), that is, a relatively low Si/Al ratio benefits the propylene productivity [177], and a high Si/Al ratio improves

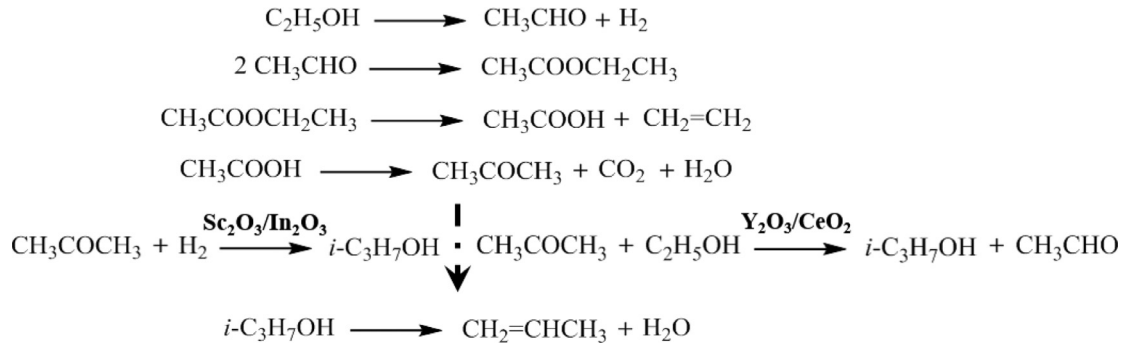


**Fig. 12.** Reaction pathways of ethanol conversion to propylene on $Sc_2O_3/In_2O_3$ and $Y_2O_3/CeO_2$ [180].

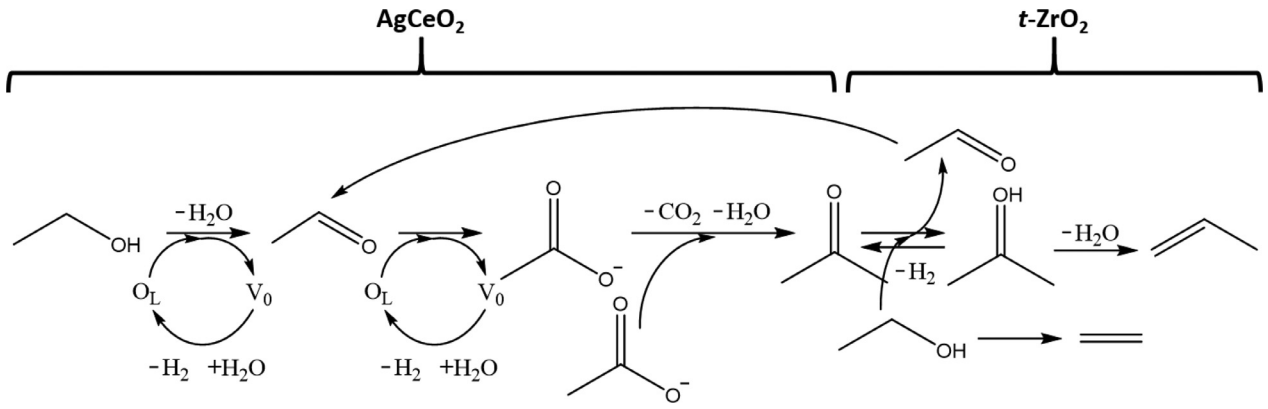


**Fig. 13.** Reaction pathways of ethanol conversion to propylene over a physical mixture of *t*-$ZrO_2$ and $AgCeO_2$. Reprinted with permission from ref [175]. Copyright (2018) American Chemical Society.

the catalytic stability [184]. The crystal size of H-ZSM-5 can also affect ethanol conversion to propylene. It was found that, based on the similar acidic property, H-ZSM-5 zeolite with smaller crystal sizes (about 100 nm) showed better propylene selectivity and stability in comparison with that with large sizes (>100 nm) [185]. It is because that small-sized zeolite has the improved accessibility and reduced diffusion path lengths, which can mitigate coke formation. Similar phenomenon was observed by Xia et al. as well, showing that a decrease in the particle size of H-ZSM-5 catalyst led to an increase in propylene yield [186]. To improve the selectivity to propylene and catalysts' stability, modified H-ZSM-5 zeolites [187,188], have been developed for ETP. The highest propylene selectivity achieved by the modified H-ZSM-5 catalysts was reported at about 30%.

$In_2O_3$ [20,180,181], $ZrO_2$ [176,189-191], and $CeO_2$ [180,183] supported metal oxides are also popular catalysts for ETP. Among them, $In_2O_3$-based catalysts ($Sc_2O_3/In_2O_3$ [180,181] and $Sc_2O_3/In_2O_3$/Beta [20]) showed the highest propylene yield of 50–62%, whilst, over the $ZrO_2$-supported catalyst ($Y_2O_3/ZrO_2$ [190,191]) and $CeO_2$-supported catalyst ($Y_2O_3/CeO_2$ [183]), the yield of propylene were about 44% and 37%, respectively. Iwamoto et al. also found that the presence of water in ethanol could decrease the coke formation and then improve the durability of $Sc_2O_3/In_2O_3$, and the addition of hydrogen increased the conversion of acetone to propylene [180,181].

In ETP reaction, propylene production is always accompanied by other olefins, especially ethylene and butylenes, which can oligomerise to higher olefins, aromatics and coke, resulting in a decrease in propylene selectivity and catalyst deactivation [192]. Therefore, the development of propylene selective catalysts is still required. It is a challenging task to obtain selective catalysts for ETP conversion because the reaction mechanism varies in the presence of different types of catalysts, and the relationships between catalyst property, activity and stability are not fully addressed. For example, for the most widely used H-ZSM-5 catalyst, the formation of ethylene (as the intermediate for propylene production) requires acid sites, but the acid sites can also catalyse the consecutive secondary reactions of ethylene and propylene to produce polyaromatics, being responsible for catalyst deactivation and low selectivity of ETP processes [179]. It is suggested that zeolite with a moderate surface acidity is preferable for the production of propylene from ethanol. Considering microporous zeolite catalysts are easily deactivated by coke deposition, reducing the catalyst crystal size and introducing mesopores into catalyst structure are the two possible routes to enhance the mass transfer and the degree of accessibility to active sites. For metal oxides and supported metal oxide catalysts, the chemical nature (acid-base property) and loading of different metals, and the types of catalyst support (increasing the surface area or providing another type of active site) have been widely studied to form a multifunctional heterogeneous catalyst to facilitate reactions with complex mechanisms, and thus to improve propylene selectivity and catalyst stability during ETP process.

### 3.3. Bioethanol to $C_4$ olefins

Isobutene and 1,3-butadiene (BD) are the main products in the conversion of ethanol to $C_4$ olefins. Isobutene is widely used in the production of polymers (*e.g.* butyl rubber) and gasoline additives (*e.g.* methyl tert-butyl ether and ethyl tert-butyl ether) [21]. Both isobutene and BD are mainly produced *via* steam cracking of naphtha, which is energy intensive and produces a mixture of $C_4$ isomers, requiring a further separation processes to obtain high purity isobutene [193,194]. To reduce the energy consumption and the use of fossil fuels, bioethanol is a sustainable feedstock to produce $C_4$ olefins.

Bioethanol can be converted to isobutene *via* a two-step process, *i.e.* converting ethanol to acetone Eqs. 24 and (25) using base metal catalysts (*e.g.* ZnO-CaO [195] and ZnO-$Fe_2O_3$ [196]), followed by the

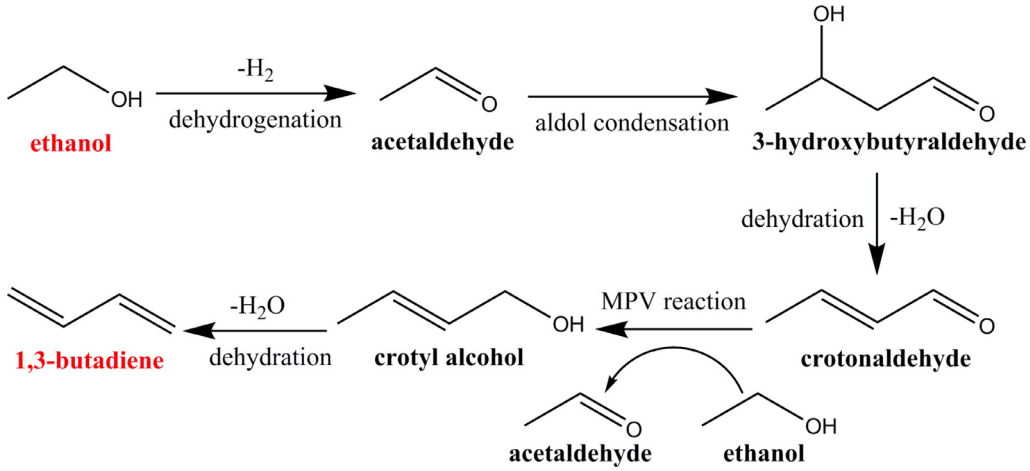


**Fig. 14.** Reaction mechanism of ethanol conversion to 1,3-butadiene [201].

transformation of acetone to isobutene (Eq. 26) on acidic zeolites (*e.g.* ZSM-5 and Beta zeolite [197]). Hence, cascade conversion of ethanol to isobutene (Eq. 27) is possible over a bifunctional catalyst with the balanced acid/base properties. $Zn_xZr_yO_z$ mixed oxide catalysts with both acidic and basic sites were then developed for the direct conversion of bioethanol to isobutene with the high yield (~83%) [198]. The catalysis over the $Zn_xZr_yO_z$ catalysts proceeded *via* a five-step sequence [199]. Ethanol first undergoes dehydrogenation to acetaldehyde followed by oxidation to produce acetic acid, which undergoes ketonisation to form acetone. Acetone then dimerises to produce diacetone alcohol (*i.e.*, condensation), which either decomposes directly to isobutene and acetic acid or produces these products by dehydration to mesityl oxide and subsequent decomposition.

$$CH_3CH_2OH \rightarrow CH_3CHO + H_2 \quad (24)$$

$$2\ CH_3CHO + H_2O \rightarrow CH_3COCH_3 + CO_2 + 2\ H_2 \quad (25)$$

$$3\ CH_3COCH_3 \rightarrow 2\ i\text{-}C_4H_8 + CO_2 + H_2O \quad (26)$$

$$3\ CH_3CH_2OH + H_2O \rightarrow i\text{-}C_4H_8 + 2\ CO_2 + 6\ H_2 \quad (27)$$

The mechanism of catalytic conversion of ethanol to BD is complex and mainly involves the following five steps (Fig. 14) [22,200,201]: (i) dehydrogenation of ethanol to acetaldehyde, (ii) aldol condensation of acetaldehyde to 3-hydroxybutyraldehyde, (iii) dehydration of 3-hydroxybutyraldehyde to crotonaldehyde, (iv) Meerwein-Ponndorf-Verley (MPV) reaction between crotonaldehyde and ethanol to obtain crotyl alcohol and (v) dehydration of crotyl alcohol to 1,3-butadiene. Therefore, being similar to ethanol conversion to isobutene, the active catalyst for converting ethanol to BD should have both acidity and basicity to enable the dehydration of crotyl alcohol to BD, and the dehydrogenation and aldol condensation reactions, respectively.

$MgO\text{-}SiO_2$ catalysts [49,202-205] containing acid-base bifunctionality have been widely studied due to their high selectivity to 1,3-butadiene (up to 87% on $MgO\text{-}SiO_2\text{-}Na_2O$). The balance of the chemical properties (*i.e.*, Mg/Si ratio) is important for the selective production of BD [49]. Other metal oxides such as $ZnO\text{-}Al_2O_3$ [206] and $Cr_2O_3\text{-}Al_2O_3$ [206] with redox properties were also developed for the conversion of ethanol to BD. Besides, silica-supported and zeolite-supported Lewis acids [207–211] were found to be highly active because these Lewis acids promoted the conversion of ethanol/acetaldehyde mixtures to BD. In addition, Ag and Cu were great promoters to enhance the formation of acetaldehyde through ethanol dehydrogenation [207,212,213].

Although BD selectivity and yield are commonly selected and used in the literature as the criteria to evaluate the catalysts' performance, from a practical point of view, BD productivity can be more appropriate. However, due to the lack of experimental details, estimation of BD productivity for a fair comparison of the catalytic performance of different catalysts can be challenging. Jones et al. suggested that a minimum target for BD productivity at 0.15 $g_{BD}\ g_{cat}^{-1}\ h^{-1}$ should be achieved before further development towards industrial application [49]. Dai et al. studied one-pot catalytic conversion of ethanol to BD over a zeolite catalyst (Zn-Y/Beta), showing an impressive BD productivity of up to 2.33 $g_{BD}\ g_{cat}^{-1}\ h^{-1}$ and a high BD selectivity of ~63%, which demonstrates the promise of the development for the potential industrial production of BD [214].

Time-on-stream (TOS) stability of the catalysts, as another crucial factor, is a long-standing challenge for ethanol-to-BD process. Catalyst deactivation due to coking is a major issue [215,216]. Pore blockage and the associated reduced accessibility of active sites by reactants/products are also the main reasons for catalyst deactivation [217]. It was found that the presence of water could significantly alleviate catalyst deactivation, which was ascribed to the inhibition of successive condensation and dehydrogenation reactions which are responsible for coke formation [218]. In addition, the use of bioethanol/water mixture as the feedstock may also reduce the operating cost since the energy-intensive removal of water from ethanol can be avoided after fermentation. Chae et al. found that mesoporous SBA-15-supported catalyst (Ta/SBA-15-100 with a pore size of 8.0 nm) had much better longevity than the catalyst based on commercial porous silica-supported (Ta/Merck with a pore size of 5.5 nm) because the large pore of SBA-15 could facilitate molecular diffusion and reduce the possibility of coking [200]. Regarding the deactivated catalysts due to coking, they can be potentially regenerated *via* calcination in air with minimum loss of catalytic activity [219,220].

## 4. Bioethanol to gasoline

Gasoline, primarily used as automotive fuel, comprises a mixture of $C_5$ to $C_{12}$ hydrocarbons [221–223]. Although ethanol-gasoline blends have been used widely, there is a limitation for the ethanol content in the blends (*e.g.*, 5–10% in the US for vehicles and 22–26% in Brazil for general use [221]) to avoid the substantial redesign of engines and filling stations due to the potential engine corrosion caused by water [24]. Currently, only flexible fuel vehicles have internal combustion engines that are capable of operating on any ethanol-gasoline blends with up to 83% ethanol content [224]. In addition, for gasoline containing ethanol, mileage per litre is not as good as that by regular gasoline because the combustion heat of ethanol (21.2 MJ/L) is lower than that of gasoline (32.5 MJ/L) [24]. Therefore, development of catalytic conversion of bioethanol to gasoline is important and promising to meet the

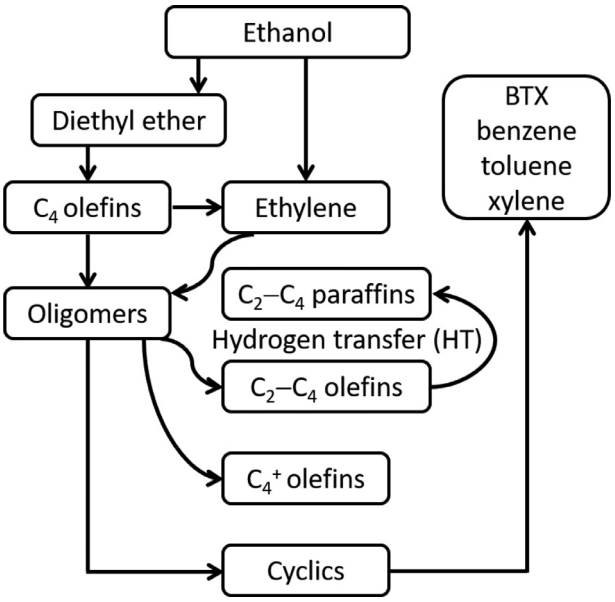


**Fig. 15.** Reaction pathways of ETG [232].

increased energy requirement while reducing the dependence on fossil fuels.

### 4.1. Catalytic reaction mechanism of ethanol-to-gasoline (ETG)

The catalytic conversion of ethanol to gasoline is complex (Fig. 15). ETG process mainly involves three steps [10,225]: ethanol dehydration to ethylene, secondary reactions (*i.e.*, oligomerisation of ethylene), and production of aromatics/paraffins through hydrogen transfer (HT). It has been demonstrated that the distribution of the hydrocarbon products in ETG is similar to that in methanol-to-gasoline (MTG) process [223,226,227], except durene (an undesired by-product from MTG process [228]), which does not occur in the products of ETG process. Acid catalysts (*e.g.*, zeolites [229] and hydroxyapatites [221]) are required for the conversion of ethanol to hydrocarbons. For ETG reaction, Brønsted acid sites are generally considered as the actives sites [165]. When Brønsted acid sites are deactivated by carbonaceous deposits, radicals generated during the reaction are identified as another type of active sites in the oligomerisation of ethylene into $C_{3+}$ hydrocarbons [230,231].

### 4.2. Catalysts for ETG reaction

Currently, there are mainly two types of solid acid catalysts used for ETG, *i.e.*, zeolites [229] and hydroxyapatites [221]. Zeolite catalysts have been extensively used and studied for ETG process in comparison with hydroxyapatite catalysts.

#### 4.2.1. Zeolite catalysts

Zeolites are the most widely used catalysts for ETG reaction. Madeira *et al.* compared the catalytic performance of three zeolites (of H-ZSM-5, H-FAU, and H-BEA) having approximately the same amount of Brønsted acid sites but having different pore structures [229]. The Brønsted acidity of H-ZSM-5, H-FAU, and H-BEA was 297, 270, and 266 μmol/g, respectively. The pore sizes of the three zeolites were around 0.55, 0.74, and 0.67 nm, respectively. Besides, the microporous volumes of them were 0.177, 0.329, and 0.271 $cm^3/g$, and the mesoporous pore volumes were 0.085, 0.141, and 0.563 $cm^3/g$, and the total pore volumes were 0.262, 0.471, and 0.835 $cm^3/g$, respectively. H-ZSM-5 zeolite with a medium pore size converted ethanol mainly to $C_{3+}$ hydrocarbons (mostly $C_5$ to $C_{11}$), whilst the large pore H-FAU and H-BEA zeolites produced mainly ethylene and diethyl ether (intermediate products). This was because that on large pore zeolites (H-FAU and H-BEA), coke molecules were aromatics and more condensed than those on H-ZSM-5. Those polyaromatic compounds rapidly blocked the porous structure of H-FAU and H-BEA and caused a significant decrease of their Brønsted acid sites. As a result, the remained acid sites on coked H-FAU and H-BEA samples were only strong enough to convert ethanol into intermediates, and the loss of strong acidity prevented the transformation of intermediates to $C_{3+}$ hydrocarbons. In contrast, the deactivation of medium pore H-ZSM-5 zeolite was slower and $C_{3+}$ hydrocarbons were mainly produced with small amounts of ethylene and diethyl ether. Similar findings were reported by Kittikarnchanaporn et al. as well [233], that is, H-ZSM-5 was highly selective to gasoline (circa (*ca.*) 93.7%), whilst HBeta and HY zeolites were not (at *ca.* 68.0% and 86.9%, respectively). Therefore, based on the findings so far, H-ZSM-5 is the most promising catalyst for promoting ETG because of its acid property and unique pore structure (or shape selectivity).

Regarding H-ZSM-5 zeolite, the main concern is the deactivation due to coke deposition and the deterioration in the acidity (*i.e.*, dealumination) of the zeolite [24,223,229]. The former is reversible, while the latter is irreversible. The coke content in the catalyst generally depends on the reaction conditions, such as reaction temperature, time-on-stream, and feed composition (particularly water content) [223]. When the coke content is low, the carbon deposits can be burned off by calcination of the catalyst at 550 °C, which does not affect the catalyst's activity significantly [24,234]. Conversely, there is a slight hysteresis in the activity-coke relationship corresponding to the reaction and regeneration steps used for the catalyst with high coke content, which may block the internal channels of the zeolite crystals (*i.e.*, the access to the active sites) [234]. The water in bioethanol has a complex effect on the catalyst deactivation [235]. It is believed that the presence of water in the feed, as well as partially as the product, mitigates catalyst deactivation by preventing coke formation at moderate temperatures (~305 °C) [235,236]. One possible reason is that water decreases the acidic strength of the catalyst by hydration of the Brønsted acid sites, and another explanation is the competitive adsorption of water and coke precursors (*e.g.*, ethylene) on the acid sites in the process of coke formation [235]. However, at high temperatures (>450 °C), the presence of water can lead to a significant loss of zeolites' active sites by dealumination, resulting in irreversible catalyst deactivation [223,234]. To minimise the effect of catalyst deactivation by the presence of water in bioethanol, a moderate reaction temperature of 300–450 °C is suggested, which requires the use of highly active catalyst. If possible, a shorter reaction time and a lower water content in the feed are preferable. Alternatively, exploring and developing water-stable catalysts for ETG reaction seem to be a promising solution. Therefore, for the catalytic upgrading of ethanol to gasoline, the desired catalyst should have good hydrothermal stability, as well as high selectivity to gasoline range hydrocarbons. To achieve the goal, modification of H-ZSM-5 has been explored, with the focus on (i) increasing the acidity of the zeolite catalysts, (ii) developing hierarchical zeolites containing mesopores and (iii) loading different metals on the zeolite catalyst.

Zeolite acidity can be varied by changing the Si/Al ratio [165] or incorporating a modifier (*e.g.*, P and La) [168,237]. A low Si/Al ratio of the zeolite catalyst (*e.g.*, 15–40 for H-ZSM-5) represents a high acidity, suggesting the high selectivity to higher hydrocarbons [146,238]. For example, Inaba et al. studied ethanol conversion over two H-ZSM-5 zeolites with Si/Al ratios of 14.5 and 95, respectively [238]. The two H-ZSM-5 catalysts achieved comparable ethanol conversions. However, the H-ZSM-5 catalyst with Si/Al = 14.5 mainly produced BTX aromatics with a selectivity of 52.9%, whilst the H-ZSM-5 catalyst with Si/Al = 95 was mainly selective to ethylene with a selectivity of 97.6%. Similar results were also reported by Chaudhuri et al. [165] and Ramasamy et al. [239]. Incorporating a modifier can also adjust the acidity of zeolite catalysts, and the loading of the modifier shows an obvious effect on the zeolite acidity. For example, when using phosphoric acid as the P source,

**Table 1**
Yield of hydrocarbon products (in wt.%) from catalytic conversion of ethanol over aluminium and transition metal exchanged ZSM-5 zeolites [241].

| Metal ion | $C_2$ | $C_{3-4}$ olefins | Paraffins | $C_{5+}$ | Aromatic hydrocarbons |
|---|---|---|---|---|---|
| $Cu^{2+}$ | 52.40 | 21.19 | 6.11 | 7.60 | 12.70 |
| $Fe^{3+}$ | 36.30 | 27.35 | 10.85 | 10.60 | 14.90 |
| $Zn^{2+}$ | 35.30 | 25.54 | 11.06 | 9.00 | 19.10 |
| $Pd^{2+}$ | 34.90 | 26.28 | 12.42 | 10.50 | 15.90 |
| $Al^{3+}$ | 32.40 | 21.21 | 19.89 | 8.40 | 18.10 |
| $Co^{2+}$ | 28.30 | 29.24 | 12.46 | 11.10 | 18.90 |
| $Mn^{2+}$ | 25.30 | 30.45 | 14.55 | 13.00 | 16.70 |
| $La^{3+}$ | 22.10 | 24.91 | 19.99 | 10.40 | 22.60 |
| $Ce^{4+}$ | 20.50 | 25.80 | 19.50 | 12.30 | 21.90 |
| $Ni^{2+}$ | 14.70 | 16.48 | 19.22 | 7.10 | 42.50 |
| $Cr^{3+}$ | 13.00 | 18.48 | 28.02 | 6.40 | 34.10 |

Zhan et al. found that the addition of 2% P into H-ZSM-5 (2% P/H-ZSM-5, 0.705 mmol/g acidity) caused a decrease of total acidity compared to parent H-ZSM-5 (0.974 mmol/g acidity) because P impregnation largely reduced the number of strong acid sites [168]. In contrast, Ramesh et al. found that the incorporation of 1.86% P into H-ZSM-5 increased the acidity from 0.56 mmol/g to 0.81 mmol/g, but a further increase of P loading to 3.72% and 7.43% significantly decreased the catalyst acidity to 0.24 and 0.22 mmol/g, respectively [237]. It was found that the impregnation of La into H-ZSM-5 catalyst could slightly enhance the total acidity (from 0.974 mmol/g for the parent H-ZSM-5 to 1.016 mmol/g for 0.5% La/H-ZSM-5), which increased the selectivity to $C_{3+}$ hydrocarbons by about 20% [168].

Mesoporosity in H-ZSM-5 zeolite is another important parameter for the effective production of gasoline from ethanol. Viswanadham et al. compared the catalytic performance of nano-crystalline and microcrystalline H-ZSM-5 zeolites, *i.e.*, H-ZSM-5(N) and H-ZSM-5(M) [232]. Both catalysts gave 100% ethanol conversion at 500°C, but the selectivity to hydrocarbons varied significantly. H-ZSM-5(N) catalyst produced 70.1% of liquid hydrocarbons as compared with 51.3% achieved by H-ZSM-5(M). The selectivity to $C_5$–$C_{10}$ paraffins was similar at ~10% for both catalysts, but H-ZSM-5(N) produced more aromatics than H-ZSM-5(M), *i.e.*, 50.6% *versus* 36.3%. Moreover, the obtained hydrocarbons by the H-ZSM-5(N) catalyst had higher research octane number (RON), *i.e.*, 95.4 *versus* 90.5, proving that H-ZSM-5(N) was more selective to the gasoline range hydrocarbons. Since both catalysts have the same Si/Al ratio of 30, and hence comparable acidity, the difference in their catalytic behaviours was ascribed to the different porosity of the two zeolites. Due to the presence of mesopores in H-ZSM-5(N), $C_{5+}$ olefins were converted to aromatics instead of propylene as in microporous H-ZSM-5(M). In the conversion of ethanol to hydrocarbons, the nano-size hierarchical H-ZSM-5 zeolite containing mesopores also demonstrated the improved catalyst lifetime as compared with the conventional catalyst due to shorter diffusion path length, faster removal of products and migration of coke precursors from the micropores to the external surface [240].

Cation exchanged zeolites (including alkali metals, alkaline earth metals, and transition metals) were developed as well for improving ethanol conversion. Schulz et al. found that only ethylene was formed by using alkali exchanged zeolites due to the loss of strong acid sites during ion exchange, prevented secondary reactions of the primary product ethylene. The exchange of ZSM-5 with alkaline earth metals or transition metals allowed the formation of a wide range of hydrocarbons (from ethylene to aromatics) [241]. Compared to alkaline earth metals, transition metals have more options (Table 1), so they have been widely studied for the catalytic conversion of ethanol to hydrocarbons.

When metals are incorporated into zeolites, the ETG process still occurs by a hydrocarbon pool mechanism (as shown in Fig. 15): the dehydration of ethanol with the subsequent oligomerisation of ethylene to form higher hydrocarbons (olefins, paraffins, and aromatics). However, it is worth to mention that some metals can inhibit the excess reactions for the formation of coke deposition, while other metals enhance the carbonisation reactions [238,242]. The incorporation of metal particles in zeolite can improve the catalyst's performance regarding ethanol conversion, selectivity to gasoline and catalyst lifetime. Borght et al. found that loading 1 wt.% of Fe, Ni, and Ga on H-ZSM-5 zeolite had a positive effect on the ethanol conversion (*i.e.*, increase from 55% to 58, 58, and 63%, respectively) due to an increase in the accessible acid sites. Ga modified H-ZSM-5 (10 wt.% Ga/H-ZSM-5) gave the highest selectivity of 73.58% to BTX aromatics compared to other metals [238]. This is because modification with Ga can enhance aromatisation reactions without blocking the catalyst pores, which possibly occurs with other metal modifiers [146,243]. Besides, $Ga_2O_3$, ZnO, and $Mo_2C$ could also promote the formation of aromatics from ethanol [244]. Additionally, it has been found that metals such as Ga and Zn [243] could increase the catalyst life, as well as altering the reaction mechanism [238]. However, the major problem associated with metal loading is the agglomeration of metal particles, especially at high metal contents, which can block the pores and even decrease the acid strength of the zeolite catalyst, resulting in a decreased performance [245]. In comparison with monometallic catalysts, bimetallic catalysts, such as Pd-Zn/MFI/$Al_2O_3$ [246] and Au-Pd/MFI/$Al_2O_3$ [242], showed the improved selectivity to $C_{3+}$ hydrocarbons.

#### 4.2.2. Hydroxyapatite (HAP) catalysts

Hydroxyapatite ($Ca_{10-x}(PO_4)_{6-x}(HPO_4)_x(OH)_{2-x}$, $x$ = 0–1) is another type of catalysts used in ETG. Since HAP catalyst contains both acid ($Ca^{2+}$) and basic ($PO_4^{3-}$ and $OH^-$) sites in a single-crystal lattice, it is expected to exhibit bifunctional properties, acting as an acid catalyst promoting ethanol dehydration reactions and as a basic catalyst promoting ethanol dehydrogenation reactions [221,222]. Tsuchida et al. firstly reported the synthesis of gasoline from bioethanol in one step over the HAP catalyst [221]. The derived gasoline with mainly $C_6$–$C_{10}$ hydrocarbons had an octane number of 99, indicating the gasoline had a good ability to withstand compression in an internal combustion engine without detonating. Carbonate hydroxyapatite (CHAP, $Ca_{10-x/2}(PO_4)_{6-x}(CO_3)_x(OH)_2$, $x$ = 0–1), obtained by substitution $PO_4^{3-}$ ions with carbonate ions ($CO_3^{2-}$), also contains both acid ($Ca^{2+}$) and basic ($PO_4^{3-}$, $CO_3^{2-}$, and $OH^-$) sites, which make it a bifunctional catalyst. CHAP was also found to be a good catalyst for direct ethanol conversion, producing a high yield (~97%) of hydrocarbon fuels (*i.e.* $C_4$–$C_{18+}$ hydrocarbons) [222].

## 5. Bioethanol to other chemicals

Ethanol can also be selectively converted to other chemicals such as acetaldehyde, diethyl ether, acetic acid, acetone, and ethyl acetate. Generally, the production of the desired products can be achieved and optimised by varying relevant process variables and the catalyst used.

Acetaldehyde is an important raw material for the production of acetic acid, 1-butanol, ethyl acetate, and crotonaldehyde. Currently, acetaldehyde is mainly produced by the direct oxidation of ethylene using homogenous palladium/copper catalysts [247,248]. Since ethylene is mainly produced from fossil fuels, the conversion of ethylene to acetaldehyde is unsustainable. In addition, to recycle and reuse homogenous palladium/copper catalysts is also rather challenging. A promising alternative is using bioethanol to replace petroleum-based ethylene for greener and more sustainable acetaldehyde production. The conversion of ethanol to acetaldehyde can be achieved *via* partial oxidation (Eq. 28) and non-oxidative direct dehydrogenation (Eq. 29) [249–251]. Ethanol partial oxidation is normally performed at low temperatures of around 200 °C due to the use of supported precious metals such as Au [247]. It is an exothermic process and produces water as by-product. As a result, separation of the resultant water from the acetaldehyde product is required if pure acetaldehyde is needed. In contrast, the direct dehydrogenation of ethanol is an endothermic process and typically con-

ducted at increased temperatures (200–300 °C) compared to the partial oxidation. Hydrogen is produced as a desirable by-product and can be easily separated and used for other applications (such as hydrogenation processes). Due to the co-production of hydrogen, direct dehydrogenation of ethanol was preferred in the early 20th century. However, the need for frequent regeneration of the ethanol dehydrogenation catalysts (typically supported Cu catalysts because of its high selectivity towards acetaldehyde [250]) pushed the partial oxidation method to be the preferred technology for the production of acetaldehyde form ethanol [251].

$Au/MgCuCr_2O_4$ is a highly active catalyst for the selective aerobic oxidation of ethanol to acetaldehyde (with 100% conversion and ~95% yield) due to the strong synergy between Au nanoparticles and surface $Cu^+$ species [247]. Au/silicalite-1, that is, encapsulated Au nanoparticles 2–3 nm in silicalite-1, was highly active and selective for the catalytic gas-phase oxidation of bioethanol to acetaldehyde, showing 50% bioethanol conversion with 98% selectivity towards acetaldehyde at 200 °C [252]. When alkali-activated USY zeolite was used as the catalyst, acetaldehyde was attained with an approximately 15-fold higher yield (50%) and with high selectivity (80%) when oxygen was co-fed with bioethanol [253]. $Ag/CeO_2$ catalyst achieved 36% bioethanol conversion with 90% acetaldehyde selectivity in the oxidation of bioethanol at 350 °C [254]. SiC-foam-structured nanocomposite catalyst $CoO@Cu_2O$ achieved 95% bioethanol conversion with 98% acetaldehyde selectivity in the gas-phase selective oxidation of bioethanol at 280 °C [255]. $Cu/ZrO_2$ catalyst is an example that achieved direct dehydrogenation of ethanol to acetaldehyde [250,256]. Hanukovich et al. found that doping Al to $ZrO_2$ support (of $Cu/ZrO_2$ catalyst) improved ethanol turnover frequency from $6 \times 10^{-3}$ $s^{-1}$ to $8 \times 10^{-2}$ $s^{-1}$ (indicating an increase in the rate of ethanol conversion to acetaldehyde) due to an increase of catalyst acidity [250]. In addition to this, $Cu\text{-}MgAlO_x$ [257] and ZnO-modified mordenite [251] have also been studied for the purpose.

$$2CH_3CH_2OH + O_2 \rightarrow 2CH_3CHO + 2H_2O$$
$$\Delta H = -204.8\,kJ/mol, \Delta G = -182.4\,kJ/mol \quad (28)$$

$$CH_3CH_2OH \rightarrow CH_3CHO + H_2 \quad \Delta H = +81.0\,kJ/mol, \Delta G = +54.8\,kJ/mol \quad (29)$$

Diethyl ether is commonly used as a solvent. Most of diethyl ether is produced as a by-product of the vapour-phase hydration of ethylene to ethanol. Alternatively, it can be synthesised on an industrial scale by the acid ether synthesis, in which ethanol is mixed with a strong acid (*e.g.*, sulphuric acid) and the resulting mixture is heated to a desired temperature (<150 °C to avoid ethylene formation). However, the use of strong acid catalysts in the process can be very corrosive. Accordingly, catalytic dehydration of ethanol over the supported catalysts, such as Cu-Fe/ZSM-5 (100% DEE selectivity) [258] and Ru/HBeta (~99% DEE selectivity) [259] zeolites, has a great potential for producing DEE. $H_2SO_4$-activated natural zeolite was used for the conversion of bioethanol (produced from fruit waste fermentation), yielding 22% of DEE at 140–160 °C for 8 h [26]. Ni/ZSM-5 catalyst has also been studied for the production of DEE from bioethanol, achieving a bioethanol conversion of 91.9% with a DEE yield of 54.7% at 230 °C [260]. In addition, no significant negative impact of water over DEE yield was observed up to an ethanol/water molar ratio of 1:1.

The primary use of acetic acid is to produce vinyl acetate monomer. At present, industrial production of acetic acid is mainly based on methanol carbonylation using Rh complex catalyst [261]. However, the separation cost to recover the precious metal catalysts from liquid phase processes can be very expensive and the separation of products is complex and energy intensive [262,263]. Fundamental studied have been carried out in the past decades for exploring the production of acetic acid from bioethanol using heterogeneous catalysts. It represents a potential sustainable route to acetic acid production because the feedstock bioethanol is produced from renewable biomass and the heterogeneous catalysts can be separated and reused.

Supported gold catalysts are considered as the most active catalysts for the oxidation of aqueous ethanol (a mimic to bioethanol) to acetic acid in the liquid phase [261,264]. Christensen et al. compared $MgAl_2O_4$-supported Pt, Pd, and Au catalysts for the oxidation of aqueous ethanol to acetic acid with air, and found that the yield of acetic acid decreased in the order of Au (83%), Pd (60%), and Pt (16%) [264]. Since then, $Au/TiO_2$ [263], $Au/SiO_2$ [265], Au/NiO [261], Au/ZnO, $Au/TiO_2$, and $Au/Al_2O_3$ [266] were also demonstrated to be active catalysts for selective oxidation of ethanol in aqueous solution (*i.e.* liquid phase). Takei et al. found that Cu-doped Au/NiO catalyst exhibited good catalytic activity with a high selectivity (>90%) towards acetic acid even at 120 °C [261]. With a slight excess of oxygen present initially, an ethanol conversion of 99.4% and a acetic acid selectivity of 99.8% could be achieved using $Au/TiO_2$ catalyst [266]. For the ethanol oxidation in the gas phase, many catalysts including Sn-Mo oxide [267], $Mo_{0.61}V_{0.31}Nb_{0.08}O_x/TiO_2$ [268] and $Ce/TiO_2$ [269] have been used and studied. For example, $Mo_{0.61}V_{0.31}Nb_{0.08}O_x/TiO_2$ catalyst achieved 100% ethanol conversion with ~95% acetic acid selectivity at 237 °C [268]. It was found that the addition of water suppressed ethanol conversion but significantly increased acetic acid selectivity [267]. This behaviour was due to the competitive adsorption of water and ethanol or adsorbed species on the catalyst's active sites. Decreasing the concentration of superficial species on the catalyst led to a decrease of ethanol conversion, and more drastically led to a decrease of secondary reaction rates, hindering the formation of by-products.

Acetone is widely used as a solvent and for the production of methyl methacrylate and bisphenol A [270]. Nowadays, acetone is produced *via* the cumene process using propylene and benzene as the feed [271]. The cumene process not only uses the fossil-based feedstock, but also shows low yields, and is energy intensive [272]. Therefore, an eco-friendly one-step process using bioethanol as the starting material (Eq. 30) has been proposed.

$$2\ CH_3CH_2OH + H_2O \rightarrow CH_3COCH_3 + CO_2 + 4\ H_2 \quad (30)$$

Murthy et al. studied the transformation of bioethanol to acetone over ZnO-, CaO-, and MnO-promoted iron oxide catalysts, and found all samples showed a comparable acetone yield of around 50% at 450 °C, which corresponded to a selectivity of ~90% [273]. However, ZnO-promoted catalyst showed the best stability (*i.e.*, the activity remained the same level as the initial activity even after 54 h usage) compared to MnO- and CaO-promoted catalysts, which deactivated rapidly after 3 h time-on-stream. Acetone was also obtained as a by-product in the catalytic steam reforming of ethanol over $CuO/CeO_2$ catalyst at 380 °C [274]. Nakajima et al. found that ZnO-CaO (with a molar ratio of 9:1) catalyst exhibited a high catalytic activity for acetone production from ethanol, showing 100% ethanol conversion and 91% acetone selectivity at 400 °C [275]. In their follow-up study, Fe-Zn mixed oxide catalyst gave 100% ethanol conversion and 94% acetone selectivity at 440 °C using for bioethanol as the feed, but acetone yield decreased by 34% after 24 h [276]. The high selectivity to acetone was obtained on a catalyst having both surface acidity and basicity, suggesting that the acid-base bifunction was needed for acetone formation from ethanol. $Cu\text{-}La_2Zr_2O_7$ catalyst achieved 96% acetone yield for the selective conversion of bioethanol to acetone at 400 °C, which was due to the acid-base properties of $La_2Zr_2O_7$ pyrochlore in addition to its relatively high surface area (45 $m^2/g$) and copper dispersion [277]. They revealed that the most plausible reaction mechanism involves ethanol dehydrogenation to acetaldehyde followed by oxidation to acetic acid and further ketonisation to yield acetone. Rodrigues et al. found that the oxidation rate of acetaldehyde was affected by the reducibility and the water dissociation activity of the catalyst [278]. The higher the reducibility and the water dissociation activity of the catalyst are, the higher the selectivity to acetone is. Therefore, acidity/basicity, reducibility and water

dissociation activity of the catalyst are important parameters for acetone synthesis from ethanol [271].

Ethyl acetate can also be obtained directly from ethanol *via* the dehydrogenative and oxidative routes [279]. The two routes have the similar reaction mechanism, that is, ethanol is firstly converted to acetaldehyde *via* non-oxidative direct dehydrogenation or partial oxidation (see details in the conversion of ethanol to acetaldehyde in the beginning of this section), and subsequently the produced acetaldehyde reacts with another ethanol or ethoxide species to form a hemiacetal, which is then dehydrogenated to ethyl acetate. The former process has already been applied to industry and it is more cost effective as compared with esterification. In this process, copper-based catalysts such as $Cu/ZnO/ZrO_2/Al_2O_3$ [280–282], Cu/*m*-$ZrO_2$ [256], $Cu/Cr_2O_3$ [283], and a physical mixture of $Cu/ZnO/Al_2O_3$ and $ZrO_2$ [279] are widely used. In the presence of $Cu/ZnO/ZrO_2/Al_2O_3$ catalyst, a high ethyl acetate selectivity of 93% was attained [281]. CuCrAl catalyst showed an ethanol conversion of about 60–65% and a selectivity to ethyl acetate of about 98.8% [25]. $CuO/Cr_2O_3$ catalyst achieved 30% ethanol conversion with 94.6% ethyl acetate selectivity when bioethanol was used as the feedstock [284]. In the case of the oxidation route, only few effort was made, in which supported PdO catalysts such as $PdO/SiO_2$ [285] and a physical mixture of PdO/*m*-$ZrO_2$ and $ZrO_2$ [279] were used. $PdO/SiO_2$ catalyst gave a ethyl acetate selectivity of around 60% [285], while a physical mixture of PdO/*m*-$ZrO_2$ and ZrO showed an ethanol conversion of approximately 45% and a ethyl acetate selectivity of around 63% [279]. Additionally, $Au/MgAl_2O_4$ and $Au/SiO_2$ catalysts were studied in the aerobic oxidation of bioethanol, it was found that ethyl acetate was the main product at ethanol concentrations of >60 wt.%, while acetic acid was mainly produced at low ethanol concentrations [263].

## 6. Conclusions and outlook

The increased availability and competitive price of bioethanol have made bioethanol valorisation attractive and promising. A wide range of commodity chemicals can be obtained from the catalytic upgrading of bioethanol, reducing the dependence on the fossil fuels and thus the associated environmental impact. In addition to the process variables (such as reaction temperature, feed composition, and residence time), catalysts play a key role in bioethanol conversion as well, determining the product selectivity and distribution during the conversion processes.

ESR is a promising route to produce hydrogen fuel. According to the reaction mechanism, desired catalysts should have the ability of water dissociation and oxidation of carbon deposits, facilitating the reaction pathways towards hydrogen. Due to the relatively high cost of noble metal catalysts, extensive study has been performed to explore and develop less-expensive transition metal catalysts, especially Ni- and/or Co-based catalysts, which exhibit excellent catalytic activity and selectivity to hydrogen. To minimise or even avoid the catalyst deactivation, supports (*e.g.*, $CeO_2$) with high oxygen mobility are preferred, which can enhance the gasification of carbon species, and thus mitigate coke formation on the catalyst. For ESR, design of catalysts with good activity and stability should mainly focus on reducing metal particle size and improving metal dispersion and metal-support interaction (such as optimisation of the catalyst preparation method and the selection of metal precursors).

For the production of ethylene from ethanol, relatively high temperature (>240 °C) is favored due to endothermicity of the reaction, whilst a promising reaction temperature for diethyl ether formation from ethanol (exothermic, $\Delta H = -25.1$ kJ/mol) is below 240 °C. Cost-effective $\gamma$-$Al_2O_3$ is a typical catalyst in ETE, but a high reaction temperature (>350 °C) is generally required to suppress reaction intermediates (mainly diethyl ether). Additionally, the use of $\gamma$-$Al_2O_3$ catalyst is also limited to high ethanol concentration in the feedstock. Zeolites with uniform pore structure and adjustable acidity are efficient catalysts for promoting ETE at low-temperatures of <300 °C. Both the pore size (by steaming treatment) and the acidity (by changing Si/Al ratio and doping modifiers) of zeolites can be easily tuned to achieve high activity. For example, 0.5%La-2%P/H-ZSM-5 achieved 100% ethanol conversion and 99.9% ethylene selectivity at 240–280 °C. Although heteropolyacid catalysts have the potential of achieving approximately 100% ethanol conversion and ethylene selectivity, they are sensitive to moisture, limiting their use in the conversion of bioethanol to ethylene.

The reaction mechanism of ETP is complex, depending greatly on the catalyst employed. Consequently, propylene production is always accompanied by other olefins, especially ethylene and butylenes, resulting in low propylene yield and selectivity. Therefore, the development of propylene-selective catalysts remains a challenge. Zeolites and supported metal oxides are widely studied catalysts in ETP. It has been demonstrated that small-sized catalyst has the improved accessibility and reduced diffusion lengths, which can mitigate coke formation. The presence of water in the feedstock can also reduce the coke formation, improving the catalyst stability.

The active catalyst for converting ethanol to $C_4$ olefins (isobutene and 1,3-butadiene) should be bifunctional with both acidic and basic sites, such as $Zn_xZr_yO_z$ and $MgO\text{-}SiO_2$ catalysts for the production of isobutene and 1,3-butadiene, respectively. In addition, redox properties also play a role in the reaction. Ag and Cu can enhance the formation of acetaldehyde through ethanol dehydrogenation, which is an important intermediate in the formation of $C_4$ olefins. The presence of water in bioethanol could significantly alleviate catalyst deactivation due to the inhibition of successive condensation and dehydrogenation reactions involved in coke formation. Mesopores of the catalyst can facilitate molecular diffusion and thus reduce the possibility of coking.

H-ZSM-5 is believed to be the most promising catalyst for ETG because of its acidic property and unique pore structure. However, H-ZSM-5 deactivate easily due to coke deposition (*i.e.*, blocking the access to the active sites) and dealumination (*i.e.*, loss of acidity). The presence of water in the system has the complex effect on catalyst deactivation. Water can prevent coke formation at moderate temperatures due to the reduced acidic strength of the catalyst by hydration of Brønsted acid sites, and the competitive adsorption of water and coke precursors on the acid sites during coke formation. In contrast, at high temperatures (> 450 °C), the presence of water can cause zeolite dealumination, leading to a great loss of catalyst's active sites. To develop catalyst with both high selectivity and hydrothermal stability for ETG, the design and modification of catalyst should focus on the regulation of the acidity and mesoporosity, as well as the addition of metal promoters.

Although fundamental research has been widely performed to enhance ethanol conversion and the selectivity towards the desired product, as well as the catalyst stability, further investigations into the catalyst structure-activity relationships and the corresponding reaction mechanisms are still required for the rational design of catalysts and efficient upgrading of bioethanol to value-added chemicals/fuels. Due to the high content of water in bioethanol crude, the influence of water on the structure and performance of catalysts and catalytic mechanisms must be critically addressed. Moreover, the associated economic implications of bioethanol valorisation should also be considered and assessed as compared with other production routes in order to enable the translation of the developed bioethanol conversions to the market.

## Declaration of Competing Interest

All authors whom contributed to this work have no conflict of interest.

## Acknowledgments

This project has received funding from the European Union's Horizon 2020 research and innovation programme under grant agree-

ment No 872102. H.X. thanks The University of Manchester President's Doctoral Scholar Award and the China Scholarship Council (file no.201606150068) for supporting her PhD research.

## References


[1] Y.Q. Li, W. Tang, Y. Chen, J.W. Liu, C.F.F. Lee, Potential of acetone-butanol-ethanol (ABE) as a biofuel, Fuel 242 (2019) 673–686.

[2] X. Wu, G. Fang, Y. Tong, D. Jiang, Z. Liang, W. Leng, L. Liu, P. Tu, H. Wang, J. Ni, X. Li, Catalytic upgrading of ethanol to n-butanol: progress in catalyst development, ChemSusChem 11 (2018) 71–85.

[3] US Department of Energy, Energy independence and security act of 2007, https://www.congress.gov/bill/110th-congress/house-bill/6, (2007).

[4] N.M. Eagan, M.D. Kumbhalkar, J.S. Buchanan, J.A. Dumesic, G.W. Huber, Chemistries and processes for the conversion of ethanol into middle-distillate fuels, Nat. Rev. Chem. 3 (2019) 223–249.

[5] J. Franco, L. Levidow, D. Fig, L. Goldfarb, M. Honicke, M.L. Mendonca, Assumptions in the European Union biofuels policy: Frictions with experiences in Germany, Brazil and Mozambique, J. Peasant Stud. 37 (2010) 661–698.

[6] REUTERS. China sets 2020 target for nationwide ethanol use to cut corn stocks, www.reuters.com/article/us-china-biofuels/china-sets-2020-target-for-nationwide-ethanol-use-tocut-corn-stocks-idUSKCN1BO03R, (2017).

[7] H. Ying, C. Phun Chien, F. Yee Van, Operational management implemented in biofuel upstream supply chain and downstream international trading: Current Issues in Southeast Asia, Energies 13 (2020).

[8] J. Kawasaki, Thapat Silalertruksa, Henry Scheyvens, Makino Yamanoshita, Environmental sustainability and climate benefits of green technology for bioethanol production in thailand, J. ISSAAS 21 (2015) 78–95.

[9] B. Sharma, C. Larroche, C.G. Dussap, Comprehensive assessment of 2G bioethanol production, Bioresour. Technol. 313 (2020) 123630.

[10] J. Sun, Y. Wang, Recent advances in catalytic conversion of ethanol to chemicals, ACS Catal 4 (2014) 1078–1090.

[11] D. Kennes, H.N. Abubackar, M. Diaz, M.C. Veiga, C. Kennes, Bioethanol production from biomass: carbohydrate *vs* syngas fermentation, J. Chem. Technol. Biotechnol. 91 (2016) 304–317.

[12] C.R. Soccol, V. Faraco, S.G. Karp, L.P.S. Vandenberghe, V. Thomaz-Soccol, A.L. Woiciechowski, A. Pandey, in: Lignocellulosic Bioethanol: Current status and future perspectives, Biofuels: Alternative Feedstocks and Conversion Processes for the Production of Liquid and Gaseous Biofuels, Academic Press, 2019, pp. 331–354.

[13] S.A. Jambo, R. Abdulla, S.H.M. Azhar, H. Marbawi, J.A. Gansau, P. Ravindra, A review on third generation bioethanol feedstock, Renew. Sustain. Energy Rev. 65 (2016) 756–769.

[14] O.J. Sanchez, C.A. Cardona, Trends in biotechnological production of fuel ethanol from different feedstocks, Bioresour. Technol. 99 (2008) 5270–5295.

[15] Y. Zhao, A. Damgaard, Y.J. Xu, S. Liu, T.H. Christensen, Bioethanol from corn stover-Global warming footprint of alternative biotechnologies, Appl. Energy 247 (2019) 237–253.

[16] Fuel ethanol production worldwide in 2020, https://www.statista.com/statistics/281606/ethanol-production-in-selected-countries/, (2021).

[17] A. Busic, N. Mardetko, S. Kundas, G. Morzak, H. Belskaya, M. Ivancic Santek, D. Komes, S. Novak, B. Santek, Bioethanol production from renewable raw materials and Its separation and purification: a review, Food Technol. Biotechnol. 56 (2018) 289–311.

[18] I. Rossetti, A. Tripodi, G. Ramis, Hydrogen, ethylene and power production from bioethanol: ready for the renewable market? Int. J. Hydrog. Energy (2019).

[19] E.V. Ovchinnikova, S.P. Banzaraktsaeva, V.A. Chumachenko, Optimal design of ring-shaped alumina catalyst: a way to intensify bioethanol-to-ethylene production in multi-tubular reactor, Chem. Eng. Res. Des. 145 (2019) 1–11.

[20] F.Q. Xue, C.X. Miao, Y.H. Yue, W. Hua, Z. Gao, $Sc_2O_3$-promoted composite of $In_2O_3$ and Beta zeolite for direct conversion of bio-ethanol to propylene, Fuel Process. Technol. 186 (2019) 110–115.

[21] B. Zhao, Y. Men, A. Zhang, J. Wang, R. He, W. An, S. Li, Influence of different precursors on isobutene production from bio-ethanol over bifunctional $Zn_1Zr_{10}Ox$ catalysts, Appl. Catal. A: Gen. 558 (2018) 150–160.

[22] X. Li, J. Pang, C. Wang, L. Li, X. Pan, M. Zheng, T. Zhang, Conversion of ethanol to 1,3-butadiene over high-performance Mg-ZrOx/MFI nanosheet catalysts via the two-step method, Green Chem 22 (2020) 2852–2861.

[23] A.D. Patel, S. Telalović, J.H. Bitter, E. Worrell, M.K. Patel, Analysis of sustainability metrics and application to the catalytic production of higher alcohols from ethanol, Catal. Today 239 (2015) 56–79.

[24] V.F. Tret'yakov, Y.I. Makarfi, K.V. Tret'yakov, N.A. Frantsuzova, R.M. Talyshinskii, The catalytic conversion of bioethanol to hydrocarbon fuel: a review and study, Catal. Ind. 2 (2011) 402–420.

[25] G. Carotenuto, R. Tesser, M. Di Serio, E. Santacesaria, Bioethanol as feedstock for chemicals such as acetaldehyde, ethyl acetate and pure hydrogen, Biomass Convers. Biorefin. 3 (2012) 55–67.

[26] W.F. Winata, K. Wijaya, A.Mara Suheryanto, W. Kurniawati, Conversion of bioethanol to diethyl ether catalyzed by sulfuric acid and zeolite, J. Indones. Chem. Soc. 3 (2020).

[27] H.T. Abdulrazzaq, T.J. Schwartz, Catalytic Conversion of Ethanol to Commodity and Specialty Chemicals, Elsevier, 2019.

[28] R.A. Dagle, A.D. Winkelman, K.K. Ramasamy, V. Lebarbier Dagle, R.S. Weber, Ethanol as a renewable building block for fuels and chemicals, Ind. Eng. Chem. Res. 59 (2020) 4843–4853.

[29] P.D. Vaidya, Y.-J. Wu, A.E. Rodrigues, Kinetics of ethanol steam reforming for hydrogen production, 2019.

[30] S. Ogo, Y. Sekine, Recent progress in ethanol steam reforming using non-noble transition metal catalysts: a review, Fuel Process. Technol. 199 (2020) 106238.

[31] H. Aitchison, R.L. Wingad, D.F. Wass, Homogeneous ethanol to butanol catalysis—Guerbet renewed, ACS Catal 6 (2016) 7125–7132.

[32] A. Galadima, O. Muraza, Catalytic upgrading of bioethanol to fuel grade biobutanol: a review, Ind. Eng. Chem. Res. 54 (2015) 7181–7194.

[33] B. Kolesinska, J. Fraczyk, M. Binczarski, M. Modelska, J. Berlowska, P. Dziugan, H. Antolak, Z.J. Kaminski, I.A. Witonska, D. Kregiel, Butanol synthesis routes for biofuel production: trends and perspectives, Materials 12 (2019).

[34] N. Sanchez, R. Ruiz, V. Hacker, M. Cobo, Impact of bioethanol impurities on steam reforming for hydrogen production: a review, Int. J. Hydrog. Energy 45 (2020) 11923–11942.

[35] R. Trane, S. Dahl, M.S. Skjøth-Rasmussen, A.D. Jensen, Catalytic steam reforming of bio-oil, Int. J. Hydrog. Energy 37 (2012) 6447–6472.

[36] L. Li, D. Tang, Y. Song, B. Jiang, Q. Zhang, Hydrogen production from ethanol steam reforming on Ni-Ce/MMT catalysts, Energy 149 (2018) 937–943.

[37] J.L. Contreras, J. Salmones, J.A. Colín-Luna, L. Nuño, B. Quintana, I. Córdova, B. Zeifert, C. Tapia, G.A. Fuentes, Catalysts for $H_2$ production using the ethanol steam reforming (a review), Int. J. Hydrog. Energy 39 (2014) 18835–18853.

[38] N. Hajjaji, Z. Khila, I. Baccar, M.-N. Pons, A thermo-environmental study of hydrogen production from the steam reforming of bioethanol, J. Energy Storage 7 (2016) 204–219.

[39] W. Fang, Y. Romani, Y. Wei, M. Jiménez-Ruiz, H. Jobic, S. Paul, L. Jalowiecki–Duhamel, Steam reforming and oxidative steam reforming for hydrogen production from bioethanol over $Mg_2AlNiXHZOY$ nano-oxyhydride catalysts, Int. J. Hydrog. Energy 43 (2018) 17643–17655.

[40] J. Vicente, J. Ereña, C. Montero, M.J. Azkoiti, J. Bilbao, A.G. Gayubo, Reaction pathway for ethanol steam reforming on a $Ni/SiO_2$ catalyst including coke formation, Int. J. Hydrog. Energy 39 (2014) 18820–18834.

[41] L.V. Mattos, G. Jacobs, B.H. Davis, F.B. Noronha, Production of hydrogen from ethanol: review of reaction mechanism and catalyst deactivation, Chem. Rev. 112 (2012) 4094–4123.

[42] C. Montero, A. Remiro, P.L. Benito, J. Bilbao, A.G. Gayubo, Optimum operating conditions in ethanol steam reforming over a $Ni/La_2O_3$-$\alpha Al_2O_3$ catalyst in a fluidized bed reactor, Fuel Process. Technol. 169 (2018) 207–216.

[43] K.I. Gursahani, R. Alcalá, R.D. Cortright, J.A. Dumesic, Reaction kinetics measurements and analysis of reaction pathways for conversions of acetic acid, ethanol, and ethyl acetate over silica-supported Pt, Appl. Catal. A: Gen. 222 (2001) 369–392.

[44] J. Kugai, S. Velu, C. Song, Low-temperature reforming of ethanol over $CeO_2$-supported Ni-Rh bimetallic catalysts for hydrogen production, Catal. Lett. 101 (2005) 255–264.

[45] J. Llorca, V.C. Corberán, N.J. Divins, R.O. Fraile, E. Taboada, Hydrogen from bioethanol, Renew. Hydrog. Technol. (2013) 135–169.

[46] J.C. Vargas, S. Ivanova, S. Thomas, A.-C. Roger, V. Pitchon, Influence of gold on Ce-Zr-Co fluorite-type mixed oxide catalysts for ethanol steam reforming, Catalysts 2 (2012) 121–138.

[47] G. Chen, J. Tao, C. Liu, B. Yan, W. Li, X. Li, Hydrogen production via acetic acid steam reforming: a critical review on catalysts, Renew. Sustain. Energy Rev. 79 (2017) 1091–1098.

[48] D.K. Liguras, D.I. Kondarides, X.E. Verykios, Production of hydrogen for fuel cells by steam reforming of ethanol over supported noble metal catalysts, Appl. Catal. B: Environ. 43 (2003) 345–354.

[49] E.V. Makshina, W. Janssens, B.F. Sels, P.A. Jacobs, Catalytic study of the conversion of ethanol into 1,3-butadiene, Catal. Today 198 (2012) 338–344.

[50] T. Hou, B. Yu, S. Zhang, T. Xu, D. Wang, W. Cai, Hydrogen production from ethanol steam reforming over $Rh/CeO_2$ catalyst, Catal. Commun. 58 (2015) 137–140.

[51] M. Cobo, D. Pieruccini, R. Abello, L. Ariza, L.F. Córdoba, J.A. Conesa, Steam reforming of ethanol over bimetallic $RhPt/La_2O_3$: long-term stability under favorable reaction conditions, Int. J. Hydrog. Energy 38 (2013) 5580–5593.

[52] P. Osorio-Vargas, C.H. Campos, R.M. Navarro, J.L.G. Fierro, P. Reyes, $Rh/Al_2O_3$-$La_2O_3$ catalysts promoted with $CeO_2$ for ethanol steam reforming reaction, J. Mol. Catal. A: Chem. 407 (2015) 169–181.

[53] A.C. Basagiannis, P. Panagiotopoulou, X.E. Verykios, Low temperature steam reforming of ethanol over supported noble metal catalysts, Top. Catal. 51 (2008) 2–12.

[54] Z. He, M. Yang, X. Wang, Z. Zhao, A. Duan, Effect of the transition metal oxide supports on hydrogen production from bio-ethanol reforming, Catal. Today 194 (2012) 2–8.

[55] I.D. González, R.M. Navarro, W. Wen, N. Marinkovic, J.A. Rodriguéz, F. Rosa, J.L.G. Fierro, A comparative study of the water gas shift reaction over platinum catalysts supported on $CeO_2$, $TiO_2$ and Ce-modified $TiO_2$, Catal. Today 149 (2010) 372–379.

[56] S.M. de Lima, A.M. da Silva, G. Jacobs, B.H. Davis, L.V. Mattos, F.B. Noronha, New approaches to improving catalyst stability over Pt/ceria during ethanol steam reforming: Sn addition and $CO_2$ co-feeding, Appl. Catal. B: Environ. 96 (2010) 387–398.

[57] J.M. Pigos, C.J. Brooks, G. Jacobs, B.H. Davis, Low temperature water-gas shift: the effect of alkali doping on the CH bond of formate over $Pt/ZrO_2$ catalysts, Appl. Catal. A: Gen. 328 (2007) 14–26.

[58] M. Martinelli, C.D. Watson, G. Jacobs, Sodium doping of Pt/*m*-$ZrO_2$ promotes C-C scission and decarboxylation during ethanol steam reforming, Int. J. Hydrog. Energy 45 (2020) 18490–18501.

[59] M.D. Marcinkowski, M.T. Darby, J. Liu, J.M. Wimble, F.R. Lucci, S. Lee, A. Michaelides, M. Flytzani-Stephanopoulos, M. Stamatakis, E.C.H. Sykes, Pt/Cu

single-atom alloys as coke-resistant catalysts for efficient C-H activation, Nat. Chem. 10 (2018) 325–332.
[60] R. Dai, Z. Zheng, W. Yan, C. Lian, X. Wu, X. An, X. Xie, Dragon fruit-like Pt-Cu@m$SiO_2$ nanocomposite as an efficient catalyst for low-temperature ethanol steam reforming, Chem. Eng. J. 379 (2020) 122299.
[61] C. Sun, Z. Zheng, S. Wang, X. Li, X. Wu, X. An, X. Xie, Yolk-shell structured Pt-$CeO_2$@Ni-$SiO_2$ as an efficient catalyst for enhanced hydrogen production from ethanol steam reforming, Ceram. Int. 44 (2018) 1438–1442.
[62] Y. Ando, Ethanol steam reforming with two-stage catalyst system for selective methane production, Int. J. Hydrog. Energy 44 (2019) 18724–18731.
[63] K. Mudiyanselage, I. Al-Shankiti, A. Foulis, J. Llorca, H. Idriss, Reactions of ethanol over $CeO_2$ and Ru/$CeO_2$ catalysts, Appl. Catal. B: Environ. 197 (2016) 198–205.
[64] A.C.W. Koh, W.K. Leong, L. Chen, T.P. Ang, J. Lin, B.F.G. Johnson, T. Khimyak, Highly efficient ruthenium and ruthenium-platinum cluster-derived nanocatalysts for hydrogen production via ethanol steam reforming, Catal. Commun. 9 (2008) 170–175.
[65] C.E. Barrios, M.V. Bosco, M.A. Baltanás, A.L. Bonivardi, Hydrogen production by methanol steam reforming: catalytic performance of supported-Pd on zinc-cerium oxides' nanocomposites, Appl. Catal. B: Environ. 179 (2015) 262–275.
[66] J.H. Lee, J.Y. Do, N.-K. Park, H.-J. Ryu, M.W. Seo, M. Kang, Hydrogen production on $Pd_{0.01}Zn_{0.29}Mg_{0.7}Al_2O_4$ spinel catalyst by low temperature ethanol steam reforming reaction, J. Energy Inst. 92 (2019) 1064–1076.
[67] J. Zhang, H. Wang, A. Dalai, Development of stable bimetallic catalysts for carbon dioxide reforming of methane, J. Catal. 249 (2007) 300–310.
[68] X. Hu, G. Lu, Inhibition of methane formation in steam reforming reactions through modification of Ni catalyst and the reactants, Green Chem 11 (2009) 724.
[69] M. Compagnoni, A. Tripodi, A. Di Michele, P. Sassi, M. Signoretto, I. Rossetti, Low temperature ethanol steam reforming for process intensification: new Ni/MxO-$ZrO_2$ active and stable catalysts prepared by flame spray pyrolysis, Int. J. Hydrog. Energy 42 (2017) 28193–28213.
[70] X. Hu, G. Lu, Comparative study of alumina-supported transition metal catalysts for hydrogen generation by steam reforming of acetic acid, Appl. Catal. B: Environ. 99 (2010) 289–297.
[71] L. He, H. Berntsen, E. Ochoa-Fernández, J.C. Walmsley, E.A. Blekkan, D. Chen, Co-Ni catalysts derived from hydrotalcite-like materials for hydrogen production by ethanol steam reforming, Top. Catal. 52 (2009) 206–217.
[72] X. You, X. Wang, Y. Ma, J. Liu, W. Liu, X. Xu, H. Peng, C. Li, W. Zhou, P. Yuan, X. Chen, Ni-Co/$Al_2O_3$ bimetallic catalysts for $CH_4$ steam reforming: elucidating the role of Co for improving coke resistance, ChemCatChem 6 (2014) 3377–3386.
[73] J. Zhang, H. Wang, A.K. Dalai, Effects of metal content on activity and stability of Ni-Co bimetallic catalysts for $CO_2$ reforming of $CH_4$, Appl. Catal. A: Gen. 339 (2008) 121–129.
[74] A. Vizcaino, P. Arena, G. Baronetti, A. Carrero, J. Calles, M. Laborde, N. Amadeo, Ethanol steam reforming on Ni/$Al_2O_3$ catalysts: effect of Mg addition, Int. J. Hydrog. Energy 33 (2008) 3489–3492.
[75] A.J. Vizcaíno, M. Lindo, A. Carrero, J.A. Calles, Hydrogen production by steam reforming of ethanol using Ni catalysts based on ternary mixed oxides prepared by coprecipitation, Int. J. Hydrog. Energy 37 (2012) 1985–1992.
[76] M.H. Youn, J.G. Seo, P. Kim, J.J. Kim, H.-I. Lee, I.K. Song, Hydrogen production by auto-thermal reforming of ethanol over Ni/$\gamma$-$Al_2O_3$ catalysts: effect of second metal addition, J. Power Sources 162 (2006) 1270–1274.
[77] C. Montero, A. Remiro, B. Valle, L. Oar-Arteta, J. Bilbao, A.G. Gayubo, Origin and nature of coke in ethanol steam reforming and its role in deactivation of Ni/$La_2O_3$-$\alpha Al_2O_3$ catalyst, Ind. Eng. Chem. Res. 58 (2019) 14736–14751.
[78] N. Pinton, M.V. Vidal, M. Signoretto, A. Martínez-Arias, V. Cortés Corberán, Ethanol steam reforming on nanostructured catalysts of Ni, Co and $CeO_2$: influence of synthesis method on activity, deactivation and regenerability, Catal. Today 296 (2017) 135–143.
[79] A. Di Michele, A. Dell'Angelo, A. Tripodi, E. Bahadori, F. Sànchez, D. Motta, N. Dimitratos, I. Rossetti, G. Ramis, Steam reforming of ethanol over Ni/$MgAl_2O_4$ catalysts, Int. J. Hydrog. Energy 44 (2019) 952–964.
[80] A.F. Cunha, Y.J. Wu, J.C. Santos, A.E. Rodrigues, Steam reforming of ethanol on copper catalysts derived from hydrotalcite-like materials, Ind. Eng. Chem. Res. 51 (2012) 13132–13143.
[81] A.F. Cunha, Y.J. Wu, F.A. Díaz Alvarado, J.C. Santos, P.D. Vaidya, A.E. Rodrigues, Steam reforming of ethanol on a Ni/$Al_2O_3$ catalyst coupled with a hydrotalcite–like sorbent in a multilayer pattern for $CO_2$ uptake, Can. J. Chem. Eng. 90 (2012) 1514–1526.
[82] C. Dang, L. Liu, G. Yang, W. Cai, J. Long, H. Yu, Mg-promoted Ni-CaO microsphere as bi-functional catalyst for hydrogen production from sorption-enhanced steam reforming of glycerol, Chem. Eng. J. 383 (2020) 123204.
[83] G. Wu, C. Zhang, S. Li, Z. Huang, S. Yan, S. Wang, X. Ma, J. Gong, Sorption enhanced steam reforming of ethanol on Ni-CaO-$Al_2O_3$ multifunctional catalysts derived from hydrotalcite-like compounds, Energy Environ. Sci. 5 (2012) 8942.
[84] C. Zhang, H. Yue, Z. Huang, S. Li, G. Wu, X. Ma, J. Gong, Hydrogen production via steam reforming of ethanol on phyllosilicate-derived Ni/$SiO_2$: enhanced metal-support interaction and catalytic stability, ACS Sustain. Chem. Eng. 1 (2012) 161–173.
[85] D. Li, L. Zeng, X. Li, X. Wang, H. Ma, S. Assabumrungrat, J. Gong, Ceria-promoted Ni/SBA-15 catalysts for ethanol steam reforming with enhanced activity and resistance to deactivation, Appl. Catal. B: Environ. 176-177 (2015) 532–541.
[86] S. Moogi, I.-G. Lee, J.-Y. Park, Effect of $La_2O_3$ and $CeO_2$ loadings on formation of nickel-phyllosilicate precursor during preparation of Ni/SBA-15 for hydrogen-rich gas production from ethanol steam reforming, Int. J. Hydrog. Energy 44 (2019) 29537–29546.
[87] S. He, S. He, L. Zhang, X. Li, J. Wang, D. He, J. Lu, Y. Luo, Hydrogen production by ethanol steam reforming over Ni/SBA-15 mesoporous catalysts: effect of Au addition, Catal. Today 258 (2015) 162–168.
[88] S. He, Z. Mei, N. Liu, L. Zhang, J. Lu, X. Li, J. Wang, D. He, Y. Luo, Ni/SBA-15 catalysts for hydrogen production by ethanol steam reforming: effect of nickel precursor, Int. J. Hydrog. Energy 42 (2017) 14429–14438.
[89] T. Nejat, P. Jalalinezhad, F. Hormozi, Z. Bahrami, Hydrogen production from steam reforming of ethanol over Ni-Co bimetallic catalysts and MCM-41 as support, J. Taiwan Inst. Chem. Eng. 97 (2019) 216–226.
[90] D. Liu, X.Y. Quek, W.N.E. Cheo, R. Lau, A. Borgna, Y. Yang, MCM-41 supported nickel-based bimetallic catalysts with superior stability during carbon dioxide reforming of methane: effect of strong metal-support interaction, J. Catal. 266 (2009) 380–390.
[91] Y. Wei, W. Cai, S. Deng, Z. Li, H. Yu, S. Zhang, Z. Yu, L. Cui, F. Qu, Efficient syngas production via dry reforming of renewable ethanol over Ni/KIT-6 nanocatalysts, Renew. Energy 145 (2020) 1507–1516.
[92] C.M.A. Parlett, A. Aydin, L.J. Durndell, L. Frattini, M.A. Isaacs, A.F. Lee, X. Liu, L. Olivi, R. Trofimovaite, K. Wilson, C. Wu, Tailored mesoporous silica supports for Ni catalysed hydrogen production from ethanol steam reforming, Catal. Commun. 91 (2017) 76–79.
[93] H. Ma, L. Zeng, H. Tian, D. Li, X. Wang, X. Li, J. Gong, Efficient hydrogen production from ethanol steam reforming over La-modified ordered mesoporous Ni-based catalysts, Appl. Catal. B: Environ. 181 (2016) 321–331.
[94] S. Mhadmhan, P. Natewong, N. Prasongthum, C. Samart, P. Reubroycharoen, Investigation of Ni/$SiO_2$ fiber catalysts prepared by different methods on hydrogen production from ethanol steam reforming, Catalysts 8 (2018) 319.
[95] V. Claude, J.G. Mahy, J. Geens, C. Courson, S.D. Lambert, Synthesis of Ni/$\gamma$-$Al_2O_3SiO_2$ catalysts with different silicon precursors for the steam toluene reforming, Microporous Mesoporous Mater 284 (2019) 304–315.
[96] S. Veiga, J. Bussi, Steam reforming of crude glycerol over nickel supported on activated carbon, Energy Convers. Manag. 141 (2017) 79–84.
[97] G. Özkan, S. Gök, G. Özkan, Active carbon-supported Ni, Ni/Cu and Ni/Cu/Pd catalysed steam reforming of ethanol for the production of hydrogen, Chem. Eng. J. 171 (2011) 1270–1275.
[98] J.Y.Z. Chiou, H.-Y. Kung, C.-B. Wang, Highly stable and active Ni-doped ordered mesoporous carbon catalyst on the steam reforming of ethanol application, J. Saudi Chem. Soc. 21 (2017) 205–209.
[99] J.-P. Cao, J. Ren, X.-Y. Zhao, X.-Y. Wei, T. Takarada, Effect of atmosphere on carbon deposition of Ni/$Al_2O_3$ and Ni-loaded on lignite char during reforming of toluene as a biomass tar model compound, Fuel 217 (2018) 515–521.
[100] M.N. Efimov, E.Y. Mironova, A.A. Vasilev, D.G. Muratov, A.A. Averin, N.A. Zhilyaeva, E.L. Dzidziguri, A.B. Yaroslavtsev, G.P. Karpacheva, Ethanol steam reforming over Co Ru nanoparticles supported on highly porous polymer-based carbon material, Catal. Commun. 128 (2019) 105717.
[101] B.L. Augusto, M.C. Ribeiro, F.J.C.S. Aires, V.T. da Silva, F.B. Noronha, Hydrogen production by the steam reforming of ethanol over cobalt catalysts supported on different carbon nanostructures, Catal. Today 344 (2020) 66–74.
[102] P.K. Seelam, M. Huuhtanen, A. Sápi, M. Szabó, K. Kordás, E. Turpeinen, G. Tóth, R.L. Keiski, CNT-based catalysts for $H_2$ production by ethanol reforming, Int. J. Hydrog. Energy 35 (2010) 12588–12595.
[103] N. Prasongthum, R. Xiao, H. Zhang, N. Tsubaki, P. Natewong, P. Reubroycharoen, Highly active and stable Ni supported on CNTs-$SiO_2$ fiber catalysts for steam reforming of ethanol, Fuel Process. Technol. 160 (2017) 185–195.
[104] A.-R. Rautio, P.K. Seelam, P. Mäki-Arvela, O. Pitkänen, M. Huuhtanen, R.L. Keiski, K. Kordas, Carbon supported catalysts in low temperature steam reforming of ethanol: study of catalyst performance, RSC Adv 5 (2015) 49487–49492.
[105] D. Chen, W. Wang, C. Liu, Ni-encapsulated graphene chainmail catalyst for ethanol steam reforming, Int. J. Hydrog. Energy 44 (2019) 6560–6572.
[106] J. Shao, G. Zeng, Y. Li, Effect of Zn substitution to a $LaNiO_{3-\delta}$ perovskite structured catalyst in ethanol steam reforming, Int. J. Hydrog. Energy 42 (2017) 17362–17375.
[107] F.N. Agüero, M.R. Morales, S. Larrégola, E.M. Izurieta, E. Lopez, L.E. Cadús, $La_{1-x}Ca_xAl_{1-y}Ni_yO_3$ perovskites used as precursors of nickel based catalysts for ethanol steam reforming, Int. J. Hydrog. Energy 40 (2015) 15510–15520.
[108] F.N. Agüero, J.A. Alonso, M.T. Fernández-Díaz, L.E. Cadus, Ni-based catalysts obtained from perovskites oxides for ethanol steam reforming, J. Fuel Chem. Technol. 46 (2018) 1332–1341.
[109] A.L.A. Marinho, R.C. Rabelo-Neto, F.B. Noronha, L.V. Mattos, Steam reforming of ethanol over Ni-based catalysts obtained from $LaNiO_3$ and $LaNiO_3$/$CeSiO_2$ perovskite-type oxides for the production of hydrogen, Appl. Catal. A: Gen. 520 (2016) 53–64.
[110] S.M. de Lima, A.M. da Silva, L.O.O. da Costa, J.M. Assaf, L.V. Mattos, R. Sarkari, A. Venugopal, F.B. Noronha, Hydrogen production through oxidative steam reforming of ethanol over Ni-based catalysts derived from $La_{1-x}CexNiO_3$ perovskite-type oxides, Appl. Catal. B: Environ. 121-122 (2012) 1–9.
[111] Y. Sekine, D. Mukai, Y. Murai, S. Tochiya, Y. Izutsu, K. Sekiguchi, N. Hosomura, H. Arai, E. Kikuchi, Y. Sugiura, Steam reforming of toluene over perovskite-supported Ni catalysts, Appl. Catal. A: Gen. 451 (2013) 160–167.
[112] L. Zhao, T. Han, H. Wang, L. Zhang, Y. Liu, Ni-Co alloy catalyst from $LaNi_{1-x}CoxO_3$ perovskite supported on zirconia for steam reforming of ethanol, Appl. Catal. B: Environ. 187 (2016) 19–29.
[113] Z. Wang, C. Wang, S. Chen, Y. Liu, Co-Ni bimetal catalyst supported on perovskite–type oxide for steam reforming of ethanol to produce hydrogen, Int. J. Hydrog. Energy 39 (2014) 5644–5652.

[114] P. Yang, N. Li, J. Teng, J. Wu, H. Ma, Effect of template on catalytic performance of $La_{0.7}Ce_{0.3}Ni_{0.7}Fe_{0.3}O_3$ for ethanol steam reforming reaction, J. Rare Earths 37 (2019) 594–601.
[115] L. Zhao, Y. Wei, Y. Huang, Y. Liu, $La_{1-x}K_xFe_{0.7}Ni_{0.3}O_3$ catalyst for ethanol steam reforming—The effect of K-doping, Catal. Today 259 (2016) 430–437.
[116] S.Q. Chen, Y.D. Li, Y. Liu, X. Bai, Regenerable and durable catalyst for hydrogen production from ethanol steam reforming, Int. J. Hydrog. Energy 36 (2011) 5849–5856.
[117] A.F. Lucredio, J.D.A. Bellido, A. Zawadzki, E.M. Assaf, Co catalysts supported on $SiO_2$ and $\gamma$-$Al_2O_3$ applied to ethanol steam reforming: effect of the solvent used in the catalyst preparation method, Fuel 90 (2011) 1424–1430.
[118] H. Song, L. Zhang, U.S. Ozkan, The effect of surface acidic and basic properties on the performance of cobalt-based catalysts for ethanol steam reforming, Top. Catal. 55 (2012) 1324–1331.
[119] J.F. Da Costa-Serra, A. Chica, Bioethanol steam reforming on Co/ITQ-18 catalyst: effect of the crystalline structure of the delaminated zeolite ITQ-18, Int. J. Hydrog. Energy 36 (2011) 3862–3869.
[120] C. Cerdá-Moreno, J.F. Da Costa-Serra, A. Chica, Co and La supported on Zn-hydrotalcite-derived material as efficient catalyst for ethanol steam reforming, Int. J. Hydrog. Energy 44 (2019) 12685–12692.
[121] T. Mondal, K.K. Pant, A.K. Dalai, Oxidative and non-oxidative steam reforming of crude bio-ethanol for hydrogen production over Rh promoted $Ni/CeO_2$-$ZrO_2$ catalyst, Appl. Catal. A: Gen. 499 (2015) 19–31.
[122] K. Robak, M. Balcerek, Review of second generation bioethanol production from residual biomass, Food Technol. Biotechnol. 56 (2018) 174–187.
[123] A.J. Akande, R.O. Idem, A.K. Dalai, Synthesis, characterization and performance evaluation of $Ni/Al_2O_3$ catalysts for reforming of crude ethanol for hydrogen production, Appl. Catal. A: Gen. 287 (2005) 159–175.
[124] M. Dan, L. Senila, M. Roman, M. Mihet, M.D. Lazar, From wood wastes to hydrogen–Preparation and catalytic steam reforming of crude bio-ethanol obtained from fir wood, Renew. Energy 74 (2015) 27–36.
[125] A.Le Valant, A. Garron, N. Bion, F. Epron, D. Duprez, Hydrogen production from raw bioethanol over $Rh/MgAl_2O_4$ catalyst: impact of impurities: heavy alcohol, aldehyde, ester, acid and amine, Catal. Today 138 (2008) 169–174.
[126] A.Le Valant, A. Garron, N. Bion, D. Duprez, F. Epron, Effect of higher alcohols on the performances of a $1\%Rh/MgAl_2O_4/Al_2O_3$ catalyst for hydrogen production by crude bioethanol steam reforming, Int. J. Hydrog. Energy 36 (2011) 311–318.
[127] F. Frusteri, G. Bonura, in: Hydrogen Production by Reforming of bio-Alcohols, Compendium of Hydrogen Energy, Woodhead Publishing, 2015, pp. 109–136.
[128] F. Frusteri, S. Freni, L. Spadaro, V. Chiodo, G. Bonura, S. Donato, S. Cavallaro, $H_2$ production for MC fuel cell by steam reforming of ethanol over MgO supported Pd, Rh, Ni and Co catalysts, Catal. Commun. 5 (2004) 611–615.
[129] I.F. Teixeira, B.T.W. Lo, P. Kostetskyy, L. Ye, C.C. Tang, G. Mpourmpakis, S.C.E. Tsang, Direct catalytic conversion of biomass-derived furan and ethanol to ethylbenzene, ACS Catal 8 (2018) 1843–1850.
[130] C.H. Bartholomew, Mechanisms of catalyst deactivation, Appl. Catal. A: Gen. 212 (2001) 17–60.
[131] J. Sehested, Four challenges for nickel steam-reforming catalysts, Catal. Today 111 (2006) 103–110.
[132] D.J. Haynes, D. Shekhawat, in: Oxidative Steam Reforming, Fuel Cells: Technologies for Fuel Processing, Elsevier, 2011, pp. 129–190.
[133] A.A. Lemonidou, P. Kechagiopoulos, E. Heracleous, S. Voutetakis, in: Steam Reforming of Bio-Oils to Hydrogen, The Role of Catalysis for the Sustainable Production of Bio-Fuels and Bio-Chemicals, Elsevier, 2013, pp. 467–493.
[134] Y.-h. Li, H.-q. Gao, J.-h. Yang, W.-l. Gao, J. Xiang, Q.-y. Li, Multi-wall carbon nanotubes supported on carbon fiber paper synthesized by simple chemical vapor deposition, Mater. Sci. Eng. B 187 (2014) 113–119.
[135] K.P. De Jong, J.W. Geus, Carbon nanofibers: catalytic synthesis and applications, Catal. Rev. 42 (2007) 481–510.
[136] G. Wang, H. Wang, W. Li, Z. Ren, J. Bai, J. Bai, Efficient production of hydrogen and multi-walled carbon nanotubes from ethanol over $Fe/Al_2O_3$ catalysts, Fuel Process. Technol. 92 (2011) 531–540.
[137] Y.C. Sharma, A. Kumar, R. Prasad, S.N. Upadhyay, Ethanol steam reforming for hydrogen production: latest and effective catalyst modification strategies to minimize carbonaceous deactivation, Renew. Sustain. Energy Rev. 74 (2017) 89–103.
[138] G. Garbarino, P. Riani, M.A. Lucchini, F. Canepa, S. Kawale, G. Busca, Cobalt-based nanoparticles as catalysts for low temperature hydrogen production by ethanol steam reforming, Int. J. Hydrog. Energy 38 (2013) 82–91.
[139] W. Mulewa, M. Tahir, N.A.S. Amin, MMT-supported $Ni/TiO_2$ nanocomposite for low temperature ethanol steam reforming toward hydrogen production, Chem. Eng. J. 326 (2017) 956–969.
[140] V. Palma, C. Ruocco, E. Meloni, A. Ricca, Highly active and stable Pt-$Ni/CeO_2$-$SiO_2$ catalysts for ethanol reforming, J. Clean. Prod. 166 (2017) 263–272.
[141] J. Bedia, R. Barrionuevo, J. Rodríguez-Mirasol, T. Cordero, Ethanol dehydration to ethylene on acid carbon catalysts, Appl. Catal. B: Environ. 103 (2011) 302–310.
[142] L. Fernández, Global price of ethylene 2017-2021, https://www.statista.com/statistics/1170573/price-ethylene-forecast-globally/, (2021).
[143] Y. Chen, Y. Wu, L. Tao, B. Dai, M. Yang, Z. Chen, X. Zhu, Dehydration reaction of bio-ethanol to ethylene over modified SAPO catalysts, J. Ind. Eng. Chem. 16 (2010) 717–722.
[144] A.P. Kagyrmanova, V.A. Chumachenko, V.N. Korotkikh, V.N. Kashkin, A.S. Noskov, Catalytic dehydration of bioethanol to ethylene: pilot-scale studies and process simulation, Chem. Eng. J. 176-177 (2011) 188–194.
[145] I. Rossetti, M. Compagnoni, E. Finocchio, G. Ramis, A. Di Michele, Y. Millot, S. Dzwigaj, Ethylene production via catalytic dehydration of diluted bioethanol: a step towards an integrated biorefinery, Appl. Catal. B: Environ. 210 (2017) 407–420.
[146] A. Galadima, O. Muraza, Zeolite catalysts in upgrading of bioethanol to fuels range hydrocarbons: a review, J. Ind. Eng. Chem. 31 (2015) 1–14.
[147] F. Roca, Catalytic dehydration of ethanol over silica-alumina, J. Catal. 14 (1969) 107–113.
[148] J.F. DeWilde, H. Chiang, D.A. Hickman, C.R. Ho, A. Bhan, Kinetics and mechanism of ethanol dehydration on $\gamma$-$Al_2O_3$: the critical role of dimer inhibition, ACS Catal 3 (2013) 798–807.
[149] M. Zhang, Y. Yu, Dehydration of ethanol to ethylene, Ind. Eng. Chem. Res. 52 (2013) 9505–9514.
[150] V.T. Deimann, Bondt and louwrenburgh, Crell. s Annalen 195 (1795) 310.
[151] D.E. Pearson, R.D. Tanner, I.D. Picciotto, J.S. Sawyer, J.H. Cleveland, Phosphoric-acid systems. 2. Catalytic conversion of fermentation ethanol to ethylene, Ind. Eng. Chem. Prod. Res. Dev. 20 (1981) 734–740.
[152] I.S. Yakovleva, S.P. Banzaraktsaeva, E.V. Ovchinnikova, V.A. Chumachenko, L.A. Isupova, Catalytic dehydration of bioethanol to ethylene, Catal. Ind. 8 (2016) 152–167.
[153] J. Li, G. Chen, J. Yan, B. Huang, H. Cheng, Z. Lou, B. Li, Solar-driven plasmonic tungsten oxides as catalyst enhancing ethanol dehydration for highly selective ethylene production, Appl. Catal. B: Environ. 264 (2020) 118517.
[154] P. Niu, X. Ren, D. Xiong, S. Ding, Y. Li, Z. Wei, X. Chen, Synthesis of highly selective and stable Co-Cr/SAPO-34 catalyst for the catalytic dehydration of ethanol to ethylene, Catalysts 10 (2020) 785.
[155] J. Haber, K. Pamin, L. Matachowski, B. Napruszewska, J. Połtowicz, Potassium and silver salts of tungstophosphoric acid as catalysts in dehydration of ethanol and hydration of ethylene, J. Catal. 207 (2002) 296–306.
[156] R. Feng, X. Hu, X. Yan, Z. Yan, M.J. Rood, A high surface area mesoporous $\gamma$-$Al_2O_3$ with tailoring texture by glucose template for ethanol dehydration to ethylene, Microporous Mesoporous Mater 241 (2017) 89–97.
[157] E.V. Ovchinnikova, L.A. Isupova, I.G. Danilova, V.V. Danilevich, B.A. Chumachenko, Study of acid-modified aluminum oxides produced by centrifugal thermal activation in dehydration of ethanol, Russ. J. Appl. Chem. 89 (2016) 683–689.
[158] P. Kostestkyy, J. Yu, R.J. Gorte, G. Mpourmpakis, Structure-activity relationships on metal-oxides: alcohol dehydration, Catal. Sci. Technol. 4 (2014) 3861–3869.
[159] S.P. Banzaraktsaeva, E.V. Ovchinnikova, V.A. Chumachenko, Dehydration of ethanol to ethylene on ring- and trilobe-shaped catalysts, Russ. J. Appl. Chem. 91 (2018) 1486–1492.
[160] S.P. Banzaraktsaeva, E.V. Ovchinnikova, I.G. Danilova, V.V. Danilevich, V.A. Chumachenko, Ethanol-to-ethylene dehydration on acid-modified ring-shaped alumina catalyst in a tubular reactor, Chem. Eng. J. 374 (2019) 605–618.
[161] M.C.H. Clemente, G.A.V. Martins, E.F. de Freitas, J.A. Dias, S.C.L. Dias, Ethylene production via catalytic ethanol dehydration by 12-tungstophosphoric acid@ceria-zirconia, Fuel 239 (2019) 491–501.
[162] G. Chen, S. Li, F. Jiao, Q. Yuan, Catalytic dehydration of bioethanol to ethylene over $TiO_2/\gamma$-$Al_2O_3$ catalysts in microchannel reactors, Catal. Today 125 (2007) 111–119.
[163] R. Le Van Mao, T.M. Nguyen, G.P. McLaughlin, The bioethanol-to-ethylene (B.E.T.E.) process, Appl. Catal. 48 (1989) 265–277.
[164] W.R. Moser, R.W. Thompson, C.C. Chiang, H. Tong, Silicon-rich H-ZSM-5 catalyzed conversion of aqueous ethanol to ethylene, J. Catal. 117 (1989) 19–32.
[165] S.N. Chaudhuri, C. Halik, J.A. Lercher, Reactions of ethanol over HZSM-5, J. Mol. Catal. 62 (1990) 289–295.
[166] R. Le Van Mao, T.M. Nguyen, J. Yao, Conversion of ethanol in aqueous solution over ZSM-5 zeolites, Appl. Catal. 61 (1990) 161–173.
[167] Q. Sheng, K. Ling, Z. Li, L. Zhao, Effect of steam treatment on catalytic performance of HZSM-5 catalyst for ethanol dehydration to ethylene, Fuel Process. Technol. 110 (2013) 73–78.
[168] N. Zhan, Y. Hu, H. Li, D. Yu, Y. Han, H. Huang, Lanthanum-phosphorous modified HZSM-5 catalysts in dehydration of ethanol to ethylene: a comparative analysis, Catal. Commun. 11 (2010) 633–637.
[169] D. Masih, S. Rohani, J.N. Kondo, T. Tatsumi, Catalytic dehydration of ethanol–to-ethylene over Rho zeolite under mild reaction conditions, Microporous Mesoporous Mater 282 (2019) 91–99.
[170] T.T. Ali, S.A. Al-Thabaiti, A.O. Alyoubi, M. Mokhtar, Copper substituted heteropolyacid catalysts for the selective dehydration of ethanol, J. Alloys Compd. 496 (2010) 553–559.
[171] J. Gurgul, M. Zimowska, D. Mucha, R.P. Socha, L. Matachowski, The influence of surface composition of $Ag_3PW_{12}O_{40}$ and $Ag_3PMo_{12}O_{40}$ salts on their catalytic activity in dehydration of ethanol, J. Mol. Catal. A: Chem. 351 (2011) 1–10.
[172] W. Alharbi, E. Brown, E.F. Kozhevnikova, I.V. Kozhevnikov, Dehydration of ethanol over heteropoly acid catalysts in the gas phase, J. Catal. 319 (2014) 174–181.
[173] V.V. Bokade, G.D. Yadav, Heteropolyacid supported on montmorillonite catalyst for dehydration of dilute bio-ethanol, Appl. Clay Sci. 53 (2011) 263–271.
[174] M. Almohalla, I. Rodríguez-Ramos, A. Guerrero-Ruiz, Comparative study of three heteropolyacids supported on carbon materials as catalysts for ethylene production from bioethanol, Catal. Sci. Technol. 7 (2017) 1892–1901.
[175] C.R.V. Matheus, L.H. Chagas, G.G. Gonzalez, E. Falabella, S. Aguiar, L.G. Appel, Synthesis of propene from ethanol: a mechanistic study, ACS Catal 8 (2018) 7667–7678.
[176] W. Xia, F. Wang, L. Wang, J. Wang, K. Chen, Highly selective lanthanum-modified zirconia catalyst for the conversion of ethanol to propylene: a combined experimental and simulation study, Catal. Lett. 150 (2019) 150–158.
[177] W. Xia, A. Takahashi, I. Nakamura, H. Shimada, T. Fujitani, Study of active sites on the MFI zeolite catalysts for the transformation of ethanol into propylene, J. Mol. Catal. A: Chem. 328 (2010) 114–118.

[178] A. Takahashi, W. Xia, Q. Wu, T. Furukawa, I. Nakamura, H. Shimada, T. Fujitani, Difference between the mechanisms of propylene production from methanol and ethanol over ZSM-5 catalysts, Appl. Catal. A: Gen. 467 (2013) 380–385.
[179] X. Li, A. Kant, Y. He, H.V. Thakkar, M.A. Atanga, F. Rezaei, D.K. Ludlow, A.A. Rownaghi, Light olefins from renewable resources: selective catalytic dehydration of bioethanol to propylene over zeolite and transition metal oxide catalysts, Catal. Today 276 (2016) 62–77.
[180] M. Iwamoto, Selective catalytic conversion of bio-ethanol to propene: a review of catalysts and reaction pathways, Catal. Today 242 (2015) 243–248.
[181] M. Iwamoto, S. Mizuno, M. Tanaka, Direct and selective production of propene from bio-ethanol on Sc-loaded $In_2O_3$ catalysts, Chemistry 19 (2013) 7214–7220.
[182] Y.I. Pyatnitsky, L.Y. Dolgikh, L.M. Senchilo, L.A. Staraya, P.E. Strizhak, Catalytic two-step process for the production of propylene from bioethanol, Theor. Exp. Chem. 55 (2019) 50–55.
[183] F. Hayashi, M. Tanaka, D. Lin, M. Iwamoto, Surface structure of yttrium-modified ceria catalysts and reaction pathways from ethanol to propene, J. Catal. 316 (2014) 112–120.
[184] W. Xia, F. Wang, X. Mu, K. Chen, A. Takahashi, I. Nakamura, T. Fujitani, Catalytic performance of H-ZSM-5 zeolites for conversion of ethanol or ethylene to propylene: effect of reaction pressure and $SiO_2/Al_2O_3$ ratio, Catal. Commun. 91 (2017) 62–66.
[185] T. Meng, D. Mao, Q. Guo, G. Lu, The effect of crystal sizes of HZSM-5 zeolites in ethanol conversion to propylene, Catal. Commun. 21 (2012) 52–57.
[186] W. Xia, K. Chen, A. Takahashi, X. Li, X. Mu, C. Han, L. Liu, I. Nakamura, T. Fujitani, Effects of particle size on catalytic conversion of ethanol to propylene over H-ZSM-5 catalysts—Smaller is better, Catal. Commun. 73 (2016) 27–33.
[187] Z. Song, A. Takahashi, I. Nakamura, T. Fujitani, Phosphorus-modified ZSM-5 for conversion of ethanol to propylene, Appl. Catal. A: Gen. 384 (2010) 201–205.
[188] Y. Furumoto, N. Tsunoji, Y. Ide, M. Sadakane, T. Sano, Conversion of ethanol to propylene over HZSM-5(Ga) co-modified with lanthanum and phosphorous, Appl. Catal. A: Gen. 417-418 (2012) 137–144.
[189] W. Xia, F. Wang, X. Mu, K. Chen, Remarkably enhanced selectivity for conversion of ethanol to propylene over $ZrO_2$ catalysts, Fuel Process. Technol. 166 (2017) 140–145.
[190] W. Xia, F. Wang, X. Mu, K. Chen, A. Takahashi, I. Nakamura, T. Fujitani, Highly selective catalytic conversion of ethanol to propylene over yttrium-modified zirconia catalyst, Catal. Commun. 90 (2017) 10–13.
[191] F. Wang, W. Xia, X. Mu, K. Chen, H. Si, Z. Li, A combined experimental and theoretical study on ethanol conversion to propylene over $Y/ZrO_2$ catalyst, Appl. Surf. Sci. 439 (2018) 405–412.
[192] N. Zhang, D. Mao, X. Zhai, Selective conversion of bio-ethanol to propene over nano-HZSM-5 zeolite: remarkably enhanced catalytic performance by fluorine modification, Fuel Process. Technol. 167 (2017) 50–60.
[193] C. Liu, J. Sun, C. Smith, Y. Wang, A study of Zn*x*Zr*y*O*z* mixed oxides for direct conversion of ethanol to isobutene, Appl. Catal. A: Gen. 467 (2013) 91–97.
[194] J. Sun, R.A. Baylon, C. Liu, D. Mei, K.J. Martin, P. Venkitasubramanian, Y. Wang, Key roles of Lewis acid-base pairs on Zn*x*Zr*y*O*z* in direct ethanol/acetone to isobutene conversion, J. Am. Chem. Soc. 138 (2016) 507–517.
[195] T. Nakajima, T. Yamaguchi, K. Tanabe, Efficient synthesis of acetone from ethanol over ZnO-CaO catalyst, J. Chem. Soc., Chem. Commun. (1987) 394–395.
[196] T. Nakajima, H. Nameta, S. Mishima, I. Matsuzaki, K. Tanabe, A highly-active and highly selective oxide catalyst for the conversion of ethanol to acetone in the presence of water-vapor, J. Mater. Chem. 4 (1994) 853–858.
[197] G.J. Hutchings, P. Johnston, D.F. Lee, C.D. Williams, Acetone conversion to isobutene in high selectivity using zeolite-Beta catalyst, Catal. Lett. 21 (1993) 49–53.
[198] J. Sun, K. Zhu, F. Gao, C. Wang, J. Liu, C.H. Peden, Y. Wang, Direct conversion of bio-ethanol to isobutene on nanosized Zn*x*Zr*y*O*z* mixed oxides with balanced acid-base sites, J. Am. Chem. Soc. 133 (2011) 11096–11099.
[199] J.E. Rorrer, F.D. Toste, A.T. Bell, Mechanism and kinetics of isobutene formation from ethanol and acetone over Zn*x*Zr*y*O*z*, ACS Catal 9 (2019) 10588–10604.
[200] H.J. Chae, T.W. Kim, Y.K. Moon, H.K. Kim, K.E. Jeong, C.U. Kim, S.Y. Jeong, Butadiene production from bioethanol and acetaldehyde over tantalum oxide-supported ordered mesoporous silica catalysts, Appl. Catal. B: Environ. 150 (2014) 596–604.
[201] Y. Zhao, S. Li, Z. Wang, S. Wang, S. Wang, X. Ma, New ZnCe catalyst encapsulated in SBA-15 in the production of 1,3-butadiene from ethanol, Chinese Chem. Lett. 31 (2020) 535–538.
[202] M. Lewandowski, G.S. Babu, M. VezzOli, M.D. Jones, R.E. Owen, D. Mattia, P. Plucinski, E. Mikolajska, A. Ochenduszko, D.C. Apperley, Investigations into the conversion of ethanol to 1,3-butadiene using $MgO:SiO_2$ supported catalysts, Catal. Commun. 49 (2014) 25–28.
[203] Q. Zhu, B. Wang, T. Tan, Conversion of ethanol and acetaldehyde to butadiene over $MgO\text{-}SiO_2$ catalysts: effect of reaction parameters and interaction between MgO and $SiO_2$ on catalytic performance, ACS Sustain. Chem. Eng. 5 (2016) 722–733.
[204] S. Da Ros, M.D. Jones, D. Mattia, M. Schwaab, E. Barbosa-Coutinho, R.C. Rabelo-Neto, F.B. Noronha, J.C. Pinto, Microkinetic analysis of ethanol to 1,3-butadiene reactions over $MgO\text{-}SiO_2$ catalysts based on characterization of experimental fluctuations, Chem. Eng. J. 308 (2017) 988–1000.
[205] R. Ohnishi, T. Akimoto, K. Tanabe, Pronounced catalytic activity and selectivity of $MgO\text{-}SiO_2\text{-}Na_2O$ for synthesis of buta-1,3-diene from ethanol, J. Chem. Soc., Chem. Commun. (1985) 1613–1614.
[206] S.K. Bhattacharyya, N.D. Ganguly, One-step catalytic conversion of ethanol to butadiene in the fixed bed. II Binary- and ternary-oxide catalyst, J. Appl. Chem. 12 (2007) 105–110.
[207] V.L. Sushkevich, Ivanova II, V.V. Ordomsky, E. Taarning, Design of a metal-promoted oxide catalyst for the selective synthesis of butadiene from ethanol, ChemSusChem 7 (2014) 2527–2536.
[208] G. Pomalaza, G. Vofo, M. Capron, F. Dumeignil, ZnTa-TUD-1 as an easily prepared, highly efficient catalyst for the selective conversion of ethanol to 1,3-butadiene, Green Chem 20 (2018) 3203–3209.
[209] G.M. Cabello González, R. Murciano, A.L. Villanueva Perales, A. Martínez, F. Vidal-Barrero, M. Campoy, Ethanol conversion into 1,3-butadiene over a mixed Hf-Zn catalyst: a study of the reaction pathway and catalyst deactivation, Appl. Catal. A: Gen. 570 (2019) 96–106.
[210] P.I. Kyriienko, O.V. Larina, S.O. Soloviev, S.M. Orlyk, S. Dzwigaj, High selectivity of TaSiBEA zeolite catalysts in 1,3-butadiene production from ethanol and acetaldehyde mixture, Catal. Commun. 77 (2016) 123–126.
[211] C. Wang, M.Y. Zheng, X.S. Li, X.Q. Li, T. Zhang, Catalytic conversion of ethanol into butadiene over high performance LiZnHf-MFI zeolite nanosheets, Green Chem 21 (2019) 1006–1010.
[212] C. Angelici, F. Meirer, A.M.J. van der Eerden, H.L. Schaink, A. Goryachev, J.P. Hofmann, E.J.M. Hensen, B.M. Weckhuysen, P.C.A. Bruijnincx, Ex situ and operando studies on the role of copper in Cu-promoted $SiO_2$-MgO catalysts for the Lebedev ethanol-to-butadiene process, ACS Catal 5 (2015) 6005–6015.
[213] V.L. Sushkevich, I.I. Ivanova, Mechanistic study of ethanol conversion into butadiene over silver promoted zirconia catalysts, Appl. Catal. B: Environ. 215 (2017) 36–49.
[214] W.L. Dai, S.S. Zhang, Z.Y. Yu, T.T. Yan, G.J. Wu, N.J. Guan, L.D. Li, Zeolite structural confinement effects enhance one-pot catalytic conversion of ethanol to butadiene, ACS Catal 7 (2017) 3703–3706.
[215] V.L. Dagle, M.D. Flake, T.L. Lemmon, J.S. Lopez, L. Kovarik, R.A. Dagle, Effect of the $SiO_2$ support on the catalytic performance of $Ag/ZrO_2/SiO_2$ catalysts for the single-bed production of butadiene from ethanol, Appl. Catal. B: Environ. 236 (2018) 576–587.
[216] T.W. Kim, J.W. Kim, S.Y. Kim, H.J. Chae, J.R. Kim, S.Y. Jeong, C.U. Kim, Butadiene production from bioethanol and acetaldehyde over tantalum oxide-supported spherical silica catalysts for circulating fluidized bed, Chem. Eng. J. 278 (2015) 217–223.
[217] M.D. Jones, C.G. Keir, C.D. Iulio, R.A.M. Robertson, C.V. Williams, D.C. Apperley, Investigations into the conversion of ethanol into 1,3-butadiene, Catal. Sci. Technol. 1 (2011) 267.
[218] G.M. Cabello González, P. Concepción, A.L. Villanueva Perales, A. Martínez, M. Campoy, F. Vidal-Barrero, Ethanol conversion into 1,3-butadiene over a mixed Hf-Zn catalyst: effect of reaction conditions and water content in ethanol, Fuel Process. Technol. 193 (2019) 263–272.
[219] J.L. Cheong, Y.L. Shao, S.J.R. Tan, X.K. Li, Y.G. Zhang, S.S. Lee, Highly active and selective Zr/MCF catalyst for production of 1,3-butadiene from ethanol in a dual fixed bed reactor system, ACS Sustain. Chem. Eng. 4 (2016) 4887–4894.
[220] T.T. Yan, L. Yang, W.L. Dai, C.M. Wang, G.J. Wu, N.J. Guan, M. Hunger, L.D. Li, On the deactivation mechanism of zeolite catalyst in ethanol to butadiene conversion, J. Catal. 367 (2018) 7–15.
[221] T. Tsuchida, T. Yoshioka, S. Sakuma, T. Takeguchi, W. Ueda, Synthesis of biogasoline from ethanol over hydroxyapatite catalyst, Ind. Eng. Chem. Res. 47 (2008) 1443–1452.
[222] J.J. Lovón-Quintana, J.K. Rodriguez-Guerrero, P.G. Valença, Carbonate hydroxyapatite as a catalyst for ethanol conversion to hydrocarbon fuels, Appl. Catal. A: Gen. 542 (2017) 136–145.
[223] A.T. Aguayo, A.G. Gayubo, A. Atutxa, M. Olazar, J. Bilbao, Catalyst deactivation by coke in the transformation of aqueous ethanol into hydrocarbons. Kinetic modeling and acidity deterioration of the catalyst, Ind. Eng. Chem. Res. 41 (2002) 4216–4224.
[224] U.S. Department of Energy (DOE), Alternative fuels data center, Flexible fuel vehicles (2018) https://afdc.energy.gov/vehicles/flexible_fuel.html.
[225] M. Krzywonos, K. Tucki, J. Wojdalski, A. Kupczyk, M. Sikora, Analysis of properties of synthetic hydrocarbons produced using the ETG method and selected conventional biofuels Made in poland in the context of environmental effects achieved, Rocz. Ochr. Sr. 19 (2017) 394–410.
[226] R. Johansson, S.L. Hruby, J. Rass-Hansen, C.H. Christensen, The hydrocarbon pool in ethanol-to-gasoline over HZSM-5 catalysts, Catal. Lett. 127 (2008) 1–6.
[227] A.T. Aguayo, A.G. Gayubo, A.M. Tarrío, A. Atutxa, J. Bilbao, Study of operating variables in the transformation of aqueous ethanol into hydrocarbons on an HZSM-5 zeolite, J. Chem. Technol. Biotechnol. 77 (2002) 211–216.
[228] E. Costa, A. Uguina, J. Aguado, P.J. Hernandez, Ethanol to gasoline process: effect of variables, mechanism, and kinetics, Ind. Eng. Chem. Process Des. Dev. 24 (1985) 239–244.
[229] F.F. Madeira, N.S. Gnep, P. Magnoux, S. Maury, N. Cadran, Ethanol transformation over HFAU, HBEA and HMFI zeolites presenting similar Bronsted acidity, Appl. Catal. A: Gen. 367 (2009) 39–46.
[230] F.F. Madeira, K. Ben Tayeb, L. Pinard, H. Vezin, S. Maury, N. Cadran, Ethanol transformation into hydrocarbons on ZSM-5 zeolites: influence of Si/Al ratio on catalytic performances and deactivation rate. Study of the radical species role, Appl. Catal. A: Gen. 443 (2012) 171–180.
[231] F.F. Madeira, N.S. Gnep, P. Magnoux, H. Vezin, S. Maury, N. Cadran, Mechanistic insights on the ethanol transformation into hydrocarbons over HZSM-5 zeolite, Chem. Eng. J. 161 (2010) 403–408.
[232] N. Viswanadham, S.K. Saxena, J. Kumar, P. Sreenivasulu, D. Nandan, Catalytic performance of nano crystalline H-ZSM-5 in ethanol to gasoline (ETG) reaction, Fuel 95 (2012) 298–304.
[233] J. Kittikarnchanaporn, T. Pairojpiriyakul, T. Boonphayoong, S. Jitkarnka, Distillate range of hydrocarbon production from bio-ethanol dehydration using HY,

HBeta, and HZSM-5 as supports of phosphorus oxide, Chem. Eng. Trans. 39 (2014) 1375–1380.
[234] A.T. Aguayo, A.G. Gayubo, A. Atutxa, B. Valle, J. Bilbao, Regeneration of a HZSM-5 zeolite catalyst deactivated in the transformation of aqueous ethanol into hydrocarbons, Catal. Today 107-108 (2005) 410–416.
[235] A.G. Gayubo, A. Alonso, B. Valle, A.T. Aguayo, M. Olazar, J. Bilbao, Kinetic modelling for the transformation of bioethanol into olefins on a hydrothermally stable Ni-HZSM-5 catalyst considering the deactivation by coke, Chem. Eng. J. 167 (2011) 262–277.
[236] J.C. Oudejans, P.F. Vandenoosterkamp, H. Vanbekkum, Conversion of ethanol over zeolite H-ZSM-5 in the presence of water, Appl. Catal. 3 (1982) 109–115.
[237] K. Ramesh, C. Jie, Y.F. Han, A. Borgna, Synthesis, characterization, and catalytic activity of phosphorus modified H-ZSM-5 catalysts in selective ethanol dehydration, Ind. Eng. Chem. Res. 49 (2010) 4080–4090.
[238] M. Inaba, K. Murata, M. Saito, I. Takahara, Ethanol conversion to aromatic hydrocarbons over several zeolite catalysts, React. Kinet. Catal. Lett. 88 (2006) 135–142.
[239] K.K. Ramasamy, Y. Wang, Ethanol conversion to hydrocarbons on HZSM-5: effect of reaction conditions and Si/Al ratio on the product distributions, Catal. Today 237 (2014) 89–99.
[240] K.K. Ramasamy, H. Zhang, J.M. Sun, Y. Wang, Conversion of ethanol to hydrocarbons on hierarchical HZSM-5 zeolites, Catal. Today 238 (2014) 103–110.
[241] J. Schulz, F. Bandermann, Conversion of ethanol over metal-exchanged zeolites, Chem. Eng. Technol. 16 (1993) 332–337.
[242] A.V. Chistyakov, P.A. Zharova, M.A. Gubanov, S.A. Nikolaev, T.B. Egorova, A.E. Gekhman, M.V. Tsodikov, Conversion of ethanol into a fraction of $C_{3+}$ hydrocarbons in the presence of gold-containing catalysts based on a zeolite MFI support, Kinet. Catal. 58 (2018) 741–748.
[243] S.K. Saha, S. Sivasanker, Influence of Zn-doping and Ga-doping on the conversion of ethanol to hydrocarbons over ZSM-5, Catal. Lett. 15 (1992) 413–418.
[244] R. Barthos, A. Szechenyi, F. Solymosi, Decomposition and aromatization of ethanol on ZSM-based catalysts, J. Phys. Chem. B 110 (2006) 21816–21825.
[245] K. Van der Borght, V.V. Galvita, G.B. Marin, Ethanol to higher hydrocarbons over Ni, Ga, Fe-modified ZSM-5: effect of metal content, Appl. Catal. A: Gen. 492 (2015) 117–126.
[246] A.V. Chistyakov, V.Y. Murzin, M.A. Gubanov, M.V. Tsodikov, Pd-Zn containing catalysts for ethanol conversion towards hydrocarbons, Chem. Eng. 32 (2013) 619–624.
[247] P. Liu, E.J. Hensen, Highly efficient and robust $Au/MgCuCr_2O_4$ catalyst for gas-phase oxidation of ethanol to acetaldehyde, J. Am. Chem. Soc. 135 (2013) 14032–14035.
[248] A. Segawa, A. Nakashima, R. Nojima, N. Yoshida, M. Okamoto, Acetaldehyde production from ethanol by eco-friendly non-chromium catalysts consisting of copper and calcium silicate, Ind. Eng. Chem. Res. 57 (2018) 11852–11857.
[249] I. Boldog, P. Čičmanec, Y. Ganjkhanlou, R. Bulánek, Surfactant templated synthesis of porous $VOx$-$ZrO_2$ catalysts for ethanol conversion to acetaldehyde, Catal. Today 304 (2018) 64–71.
[250] S. Hanukovich, A. Dang, P. Christopher, Influence of metal oxide support acid sites on Cu-catalyzed nonoxidative dehydrogenation of ethanol to acetaldehyde, ACS Catal 9 (2019) 3537–3550.
[251] S.J. Raynes, R.A. Taylor, Zinc oxide-modified mordenite as an effective catalyst for the dehydrogenation of (bio)ethanol to acetaldehyde, Sustain. Energy Fuels 5 (2021) 2136–2148.
[252] J. Mielby, J.O. Abildstrom, F. Wang, T. Kasama, C. Weidenthaler, S. Kegnaes, Oxidation of bioethanol using zeolite-encapsulated gold nanoparticles, Angew. Chem. Int. Ed. Engl. 53 (2014) 12513–12516.
[253] G.M. Lari, K. Desai, C. Mondelli, J. Pérez-Ramírez, Selective dehydrogenation of bioethanol to acetaldehyde over basic USY zeolites, Catal. Sci. Technol. 6 (2016) 2706–2714.
[254] P.H. Rana, P.A. Parikh, Bioethanol selective oxidation to acetaldehyde over $Ag–CeO_2$: role of metal–support interactions, New J. Chem. 41 (2017) 2636–2641.
[255] G. Zhao, S. Fan, X. Pan, P. Chen, Y. Liu, Y. Lu, Reaction-induced self-assembly of $CoO@Cu_2O$ nanocomposites in situ onto SiC-foam for gas-phase oxidation of bioethanol to acetaldehyde, ChemSusChem 10 (2017) 1380–1384.
[256] A.G. Sato, D.P. Volanti, D.M. Meira, S. Damyanova, E. Longo, J.M.C. Bueno, Effect of the $ZrO_2$ phase on the structure and behavior of supported Cu catalysts for ethanol conversion, J. Catal. 307 (2013) 1–17.
[257] I.S.P. Campisano, C.B. Rodella, Z.S.B. Sousa, C.A. Henriques, V. Teixeira da Silva, Influence of thermal treatment conditions on the characteristics of Cu-based metal oxides derived from hydrotalcite-like compounds and their performance in bio-ethanol dehydrogenation to acetaldehyde, Catal. Today 306 (2018) 111–120.
[258] T.K.R. de Oliveira, M. Rosset, O.W. Perez-Lopez, Ethanol dehydration to diethyl ether over Cu-Fe/ZSM-5 catalysts, Catal. Commun. 104 (2018) 32–36.
[259] T. Kamsuwan, P. Praserthdam, B. Jongsomjit, Diethyl ether production during catalytic dehydration of ethanol over Ru- and Pt- modified H-beta eeolite catalysts, J. Oleo Sci. 66 (2017) 199–207.
[260] D.T. Sarve, S.K. Singh, J.D. Ekhe, Kinetic and mechanistic study of ethanol dehydration to diethyl ether over Ni-ZSM-5 in a closed batch reactor, React. Kinet. Mech. Catal. 131 (2020) 261–281.
[261] T. Takei, N. Iguchi, M. Haruta, Synthesis of acetoaldehyde, acetic acid, and others by the dehydrogenation and oxidation of ethanol, Catal. Surv. Asia 15 (2011) 80–88.
[262] N. Yoneda, S. Kusano, M. Yasui, P. Pujado, S. Wilcher, Recent advances in processes and catalysts for the production of acetic acid, Appl. Catal. A: Gen. 221 (2001) 253–265.
[263] B. Jorgensen, S. Egholmchristiansen, M. Dahlthomsen, C. Christensen, Aerobic oxidation of aqueous ethanol using heterogeneous gold catalysts: efficient routes to acetic acid and ethyl acetate, J. Catal. 251 (2007) 332–337.
[264] C.H. Christensen, B. Jørgensen, J. Rass-Hansen, K. Egeblad, R. Madsen, S.K. Klitgaard, S.M. Hansen, M.R. Hansen, H.C. Andersen, A. Riisager, Formation of acetic acid by aqueous-phase oxidation of ethanol with air in the presence of a heterogeneous gold catalyst, Angew. Chem. 118 (2006) 4764–4767.
[265] K.-Q. Sun, S.-W. Luo, N. Xu, B.-Q. Xu, Gold nano-size effect in $Au/SiO_2$ for selective ethanol oxidation in aqueous solution, Catal. Lett. 124 (2008) 238–242.
[266] S.M. Tembe, G. Patrick, M.S. Scurrell, Acetic acid production by selective oxidation of ethanol using Au catalysts supported on various metal oxide, Gold Bull 42 (2009) 321–327.
[267] P.R.S. Medeiros, J.G. Eon, L.G. Appel, The role of water in ethanol oxidation over $SnO_2$-supported molybdenum oxides, Catal. Lett. 69 (2000) 79–82.
[268] X. Li, E. Iglesia, Selective catalytic oxidation of ethanol to acetic acid on dispersed Mo-V-Nb mixed oxides, Chemistry 13 (2007) 9324–9330.
[269] Y. Eguchi, D. Abe, H. Yoshitake, Oxidation state of Ce and ethanol–oxygen reaction of mesoporous titania-supported cerium oxide, Microporous Mesoporous Mater 116 (2008) 44–50.
[270] L.d.R. Silva-Calpa, P.C. Zonetti, D.C. de Oliveira, R.R. de Avillez, L.G. Appel, Acetone from ethanol employing $ZnxZr_{1-}x\ O_{2-}y$, Catal. Today 289 (2017) 264–272.
[271] C.P. Rodrigues, P.D.C. Zonetti, L.G. Appel, Chemicals from ethanol: the acetone synthesis from ethanol employing $Ce_{0.75}Zr_{0.25}O_2$, $ZrO_2$ and $Cu/ZnO/Al_2O_3$, Chem. Cent. J. 11 (2017) 30.
[272] S. Niwa Si, M. Eswaramoorthy, J. Nair, A. Raj, N. Itoh, H. Shoji, T. Namba, F. Mizukami, A one-step conversion of benzene to phenol with a palladium membrane, Science 295 (2002) 105–107.
[273] R. Murthy, Conversion of ethanol to acetone over promoted iron oxide catalysis, J. Catal. 109 (1988) 298–302.
[274] T. Nishiguchi, T. Matsumoto, H. Kanai, K. Utani, Y. Matsumura, W.J. Shen, S. Imamura, Catalytic steam reforming of ethanol to produce hydrogen and acetone, Appl. Catal. A: Gen. 279 (2005) 273–277.
[275] T. Nakajima, T. Yamaguchi, K. Tanabe, Efficient synthesis of acetone from ethanol over ZnO–CaO catalyst, J. Chem. Soc., Chem. Commun. (1987) 394–395.
[276] T. Nakajima, H. Nameta, S. Mishima, I. Matsuzaki, K. Tanabe, A highly active and highly selective oxide catalyst for the conversion of ethanol to acetone in the presence of water vapour, J. Mater. Chem. 4 (1994).
[277] J. Bussi, S. Parodi, B. Irigaray, R. Kieffer, Catalytic transformation of ethanol into acetone using copper–pyrochlore catalysts, Appl. Catal. A: Gen. 172 (1998) 117–129.
[278] C.P. Rodrigues, P.C. Zonetti, C.G. Silva, A.B. Gaspar, L.G. Appel, Chemicals from ethanol—The acetone one-pot synthesis, Appl. Catal. A: Gen. 458 (2013) 111–118.
[279] A.B. Gaspar, F.G. Barbosa, S. Letichevsky, L.G. Appel, The one-pot ethyl acetate syntheses: the role of the support in the oxidative and the dehydrogenative routes, Appl. Catal. A: Gen. 380 (2010) 113–117.
[280] K. Inui, T. Kurabayashi, S. Sato, Direct synthesis of ethyl acetate from ethanol over Cu-Zn-Zr-Al-O catalyst, Appl. Catal. A: Gen. 237 (2002) 53–61.
[281] K. Inui, T. Kurabayashi, S. Sato, Direct synthesis of ethyl acetate from ethanol carried out under pressure, J. Catal. 212 (2002) 207–215.
[282] K. Inui, T. Kurabayashi, S. Sato, N. Ichikawa, Effective formation of ethyl acetate from ethanol over Cu-Zn-Zr-Al-O catalyst, J. Mol. Catal. A: Chem. 216 (2004) 147–156.
[283] S. Colley, J. Tabatabaei, K. Waugh, M. Wood, The detailed kinetics and mechanism of ethyl ethanoate synthesis over a $Cu/Cr_2O_3$ catalyst, J. Catal. 236 (2005) 21–33.
[284] N.T. Hong Thuy, Y. Kikuchi, H. Sugiyama, M. Noda, M. Hirao, Techno-economic and environmental assessment of bioethanol-based chemical process: a case study on ethyl acetate, Environ. Prog. Sustain. Energy 30 (2011) 675–684.
[285] A.B. Gaspar, A.M.L. Esteves, F.M.T. Mendes, F.G. Barbosa, L.G. Appel, Chemicals from ethanol-The ethyl acetate one-pot synthesis, Appl. Catal. A: Gen. 363 (2009) 109–114.